Toward Socially Aware Robot Navigation in Dynamic and Crowded Environments: A Proactive Social Motion Model

Xuan-Tung Truong and Trung Dung Ngo, *Member, IEEE*

***Abstract*— Safe and social navigation is the key to deploying a mobile service robot in a human-centered environment. Widespread acceptability of mobile service robots in daily life is hindered by robot's inability to navigate in crowded and dynamic human environments in a socially acceptable way that would guarantee human safety and comfort. In this paper, we propose an effective proactive social motion model (PSMM) that enables a mobile service robot to navigate safely and socially in crowded and dynamic environments. The proposed method considers not only human states (position, orientation, motion, field of view, and hand poses) relative to the robot but also social interactive information about human–object and human group interactions. This allows development of the PSMM that consists of elements of an extended social force model and a hybrid reciprocal velocity obstacle technique. The PSMM is then combined with a path planning technique to generate a motion planning system that drives a mobile robot in a socially acceptable manner and produces respectful and polite behaviors akin to human movements.**

***Note to Practitioners*—In this paper, we validated the effectiveness and feasibility of the proposed proactive social motion model (PSMM) through both simulation and real-world experiments under the newly proposed human comfortable safety indices. To do that, we first implemented the entire navigation system using the open-source robot operating system. We then installed it in a simulated robot model and conducted experiments in a simulated shopping mall-like environment to verify its effectiveness. We also installed the proposed algorithm on our mobile robot platform and conducted experiments in our office-like laboratory environment. Our results show that the developed socially aware navigation framework allows a mobile robot to navigate safely, socially, and proactively while guaranteeing human safety and comfort in crowded and dynamic environments.**

In this paper, we examined the proposed PSMM with a set of predefined parameters selected based on our empirical experiences about the robot mechanism and selected social environment. However, in fact a mobile robot might need to adapt to various contextual and cultural situations in different social environments. Thus, it should be equipped with an online adaptive interactive learning mechanism allowing the robot to learn to auto-adjust their parameters according to such embedded environments. Using machine learning techniques, e.g., inverse reinforcement learning [1] to optimize the parameter set for the PSMM could be a promising research direction to improve adaptability of mobile service robots in different social environments.

In the future, we will evaluate the proposed framework based on a wider variety of scenarios, particularly those with different social interaction situations and dynamic environments. Furthermore, various kinds of social cues and signals introduced in [2] and [3] will be applied to extend the proposed framework in more complicated social situations and contexts. Last but not least, we will investigate different machine learning techniques and incorporate them in the PSMM in order to allow the robot to automatically adapt to diverse social environments.

***Index Terms*— Human comfortable safety, mobile service robots, proactive social motion model (PSMM), social robots, socially aware robot navigation.**

Manuscript received August 16, 2016; revised March 26, 2017; accepted July 9, 2017. This paper was recommended for publication by Associate Editor S. Carpin and Editor D. Tilbury upon evaluation of the reviewers' comments. *(Corresponding author: Xuan-Tung Truong.)*

X.-T. Truong is with the Faculty of Science, University of Brunei Darussalam, Bandar Seri Begawan BE1410, Brunei, and also with the Faculty of Control Engineering, Le Quy Don Technical University, Hanoi 10000, Vietnam (e-mail: xuantung.truong@gmail.com).

T. D. Ngo is with the Faculty of Science, University of Brunei Darussalam, Bandar Seri Begawan BE1410, Brunei, and also with the More-Than-One Robotics Laboratory, School of Sustainable Design Engineering, University of Prince Edward Island, Charlottetown, PE C1A 4P3, Canada (e-mail: dungnt@ieee.org).

Color versions of one or more of the figures in this paper are available online at http://ieeexplore.ieee.org.

Digital Object Identifier 10.1109/TASE.2017.2731371

I. Introduction

THE ability to autonomously navigate in human and dynamic environments, such as museums [4], airports [5], offices and the home [6], shopping malls [7], and urban environments [8], is crucial for mobile service robots. If we wish to deploy the robots in such social environments, the first and most important issue is that the robot must avoid not only regular obstacles but also humans while navigating safely toward a given goal. In this context, human safety as regards robot navigation can be classified into two categories [9]: 1) physical safety and 2) psychological safety. The first category—the most obvious issue—is to maintain a minimum physical distance between the robot and humans. The second category in the context of human–robot social interaction implies that the mobile robot is not allowed to cause stress and discomfort to humans during its navigation and interaction.

Regarding the physical aspect of safety, conventional mobile robot navigation systems usually consider humans as regular obstacles such that collision avoidance techniques can be applied. Several obstacle avoidance and motion control methods such as the artificial potential field [10], vector field histogram [11], dynamic window approach [12], velocity obstacles (VOs) [13], randomized kinodynamic planning [14], [15], inevitable collision states [16], and reciprocal VOs (RVOs) [17] techniques have been proposed. These approaches have been evaluated such that robots are capable of planning their trajectories to avoid undesired physical contact

with humans. However, none of these methods goes beyond the physical safety aspects to address the psychological safety aspects, including human characteristics and social constraints.

To guarantee both physical and psychological safety, recent research on human-aware robot navigation systems [18], [19] has aimed to create more socially acceptable behaviors for mobile robots. Some of these have been applied to real-world environments and have achieved considerable success. The existing navigation techniques, however, suffer some drawbacks. First, the navigation system deals only with interactions with a single human, making it difficult to apply such a system to a real-world environment, where groups of humans are more common [20]. Hence, such developed navigation systems lack robustness in diverse social situations. Second, the author applied 2-D costmaps and path planning-based approach, and thus it is difficult to apply in crowded environments, because of the higher computational cost. Finally, these techniques address only the issue in the sparse and semidynamic environment; therefore, it is difficult to apply in the dynamic and crowded environments.

To overcome the above-mentioned weaknesses of the conventional mobile robot navigation system and enhance the navigability of mobile service robot in crowded and dynamic human environments, we proposed a new system architecture of mobile robot navigation in dynamic and crowded environments. Specifically, based on the conventional navigation scheme [21], we have developed a socially aware navigation framework by extracting human features from the socio-spatiotemporal characteristics of individuals and human groups, and then incorporating that information into the robot navigation system. In the new architecture, we have developed an extended social force model (ESFM) based on the conventional social force model (SFM) [22] and integrated human information into the hybrid RVO (HRVO) [23]. After that, we have incorporated advantages of the ESFM model and the HRVO into the proactive social motion model (PSMM) for mobile robot in dynamic and crowded environments. In addition, we have developed human comfortable safety indices (HCSIs) including social individual index (SII), social group index (SGI), and relative motion index (RMI) to evaluate the proposed framework. We have demonstrated the effectiveness of the proposed model through statistical data from simulations and real-world experiments, and evaluated the results using the proposed HCSIs. Through results of simulations and real experiments, we proved that the proposed framework overcomes the shortcomings of the conventional mobile robot navigation systems while guaranteeing both physical and psychological safety of human coworkers in crowded and dynamic workspaces. Specially, this method can be used with any local and global path planning method (even those with given waypoints) to navigate mobile robots toward their destinations. The remainder of this paper is organized as follows. Section II describes literature regarding human-aware robot navigation. Section III presents the proposed proactive social motion control. Section IV addresses how to integrate the socially aware robot navigation framework into the motion planning system of a differential-drive mobile robot. Section V presents the newly proposed HCSIs used to measure both the physical and psychological safety of humans, and socially acceptable behaviors of the mobile robot. Sections VI and VII show the simulation and experimental results, respectively. We provide remarks and the conclusion of this paper in Section VIII.

II. Related Works

Social environments are dynamic, uncertain, clustered, and even crowded environments with the presence of humans. Therefore, in order to ensure the human safety and comfort in such environments, several human-aware mobile robot navigation systems [5], [24], [18], [19], [25], [26] have been proposed in recent years. In this section, we review two research topics associated with the human-aware robot navigation systems in dynamic and crowded environments: 1) *human information*-based human-aware mobile robot navigation systems and 2) *navigation techniques*-based approaches. The former involves the human information incorporated into the robot navigation system, while the latter covers techniques applied to develop the robot navigation system.

The *human information*-based human-aware mobile robot navigation systems can be divided into two categories: 1) *individual state information* and 2) *social interaction information*. Individual state information (e.g., human position, orientation, motion, and field of view) is identified in the former, while human–object interaction and human group state information is in the latter.

The conventional human-aware mobile robot navigation systems are mostly based on individual state information. Trautman *et al*. [27] proposed a human–robot cooperation model for mobile robot navigation using a multiple goal interacting Gaussian process. Although this proposed method enables the mobile robot to navigate safely and efficiently in dense human crowds, it does not take social human group interaction into account; thus, under this model, the mobile robot navigation system acts according to individual states only. Chi-Pang *et al*. [28] introduced human-centered sensitive navigation using human position and motion states. This method proposed six harmonious rules that the robot has to follow to guarantee human physical safety and socially acceptable paths in the presence of humans and other robots. The method was developed based on human position and motion, but it does not consider human social group information.

A few mobile robot navigation systems have been developed by taking both individual states and human group information into consideration, but most of them are still in the early stages of development. Rios-Martinez *et al*. [29] proposed a risk-based navigation algorithm for mobile robot navigation in dynamic populated environments. Although the personal space [30] and O-space [31] concepts are taken into account to model the space around the humans, the system only takes into account groups of two standing people. Gomez *et al*. [32] presented a personal space model for both individuals and human groups using a mixture of two Gaussian functions, and developed six different subproblems of social path planning using a fast-matching squares method. However, this paper incorporates only a single static human, without considering information about human social groups.

The *navigation techniques*-based human-aware mobile robots can be roughly classified into two groups: 1) 2-D costmap-based methods and 2) reactive control-based techniques. In the first group, 2-D Gaussian or linear techniques are used to model the space around the humans—i.e., social costmaps—such that these costmaps can be used to guide the motion of a mobile robot. In the second group, obstacle avoidance algorithms are to avoid collision with human obstacles in the vicinity of the robot. The costmaps model imports the socio-spatiotemporal characteristics of humans into a local path planner to generate a feasible path for the robot that satisfies socially acceptable behaviors [33], [34]. However, this approach is time consuming, and it is highly computationally difficult to find a feasible path in crowded and dynamic environments [25], [26]. In contrast, the SFM is a useful way to drive a mobile robot in high density conditions because of its reasonable computational costs [22], [35]. Social cues and social signals can be incorporated into the motion model, such as face orientation [36]. However, this method does not explicitly deal with potential collisions in which the robot might cause humans discomfort, thereby violating human psychological safety. The RVO, based on VOs [13], takes into account the motions of nearby humans and other objects, but again it is difficult to incorporate social constraints directly into this model. Furthermore, these human-aware navigation techniques based on costmaps, SFM, and RVO only deal with human features and characteristics extracted from a single person rather than the social characteristics and constraints of human interactive information such as human–object and human group interactions, which are more common in social environments [20]. Hence, such developed navigation systems lack robustness in diverse social situations.

Several 2-D costmap-based human-aware robot navigation algorithms have been proposed to generate socially acceptable behaviors for mobile robots [26], [33], [34], [37], [38]. In [33], a generalized framework for representing social conventions, such as the concept of personal space and rules designating directional paths to either side of a hallway or set of stairs, is used for path planning and motion control. These social conventions are modeled as costmaps, and the A* planner is applied to generate a path. However, this framework has only been implemented and verified in simulation. Sisbot *et al*. [34] proposed a human-aware mobile robot motion planner to generate safe and socially acceptable paths. An extension of this system with two additional blocks, including perspective placement and a trajectory planner, was also proposed in [37]. Although the framework takes human position, human field of view, and human postures into account, it does not consider human motion or human group information. In [38], a complicated model of personal space was presented, where four different Gaussian functions were integrated to develop the robot's motion control. In this approach, however, the mobile robot is able to detect only a single-person situation, and perceives the real-world environment as a 2-D image captured by a laser range finder. Lu and Smart [26] proposed an efficient navigation framework for mobile robots navigating in a corridor using social cues. In this system, human postures and gaze behaviors are taken into account to model the socially aware costmaps around humans. These costmaps are then used to guide the robot to avoid humans during robot navigation.

The reactive control-based human-aware mobile robot navigation systems can also be divided into two subgroups: 1) potential field-based approaches and 2) VOs-based techniques. In the former, the SFM is used to develop the motion model of the mobile robots. In the later, the HRVO model is applied to design the motion control of the mobile robots.

Recently, some algorithms [35], [36], [39] have been proposed for human-aware mobile robot navigation using the SFM introduced in [22]. Despite the fact that these techniques have been able to generate socially acceptable behaviors for mobile robots, they do not proactively deal with different social situations in crowded environments such as socially avoiding human group interaction or human–object interaction. Ferrer *et al*. [35] presented a robot companion using the SFM for human-aware mobile robot navigation in an urban environment. An interactive learning is also used to adjust the parameters of the proposed model and ensure that the system works correctly and smoothly. Ratsamme *et al*. [36] proposed a human–robot collision avoidance technique based on an ESFM modified from the conventional SFM [22] using additional human factors including body pose, face orientation, and personal space. The model is then used to predict human motion and perform human–robot collision avoidance. Shiomi *et al*. [39] presented a socially acceptable collision avoidance technique for a mobile robot navigating among pedestrians. The modified SFM introduced in [40] was used to model pedestrian motion and to develop human-like collision avoidance. Although the robot provides safe and comfortable collision avoidance behaviors toward humans, the technique has been verified only in single-human situations.

More recently, a few human-aware robot navigation systems [41], [42] based on the RVOs technique [17], [43] have been proposed. Although these methods have been successfully verified in a real-world environment, they might not be able to handle all social situations and they are still in an early stage of development. Zhang *et al*. [41] proposed a local collision avoidance method using the optimal reciprocal collision avoidance system introduced in [43]. To reduce the uncertainties in the state estimation process of pedestrians and the robot, the encircling particle method is used. Daniel *et al*. [42] presented a human-safe navigation algorithm using the VOs paradigm introduced in [23]. Instead of choosing the optimal velocity based on the preferred velocity space, the authors used Monte Carlo sampling throughout the velocity space and evaluated the samples by incorporating factors of differing importance consisting of humans, other robots, and obstacles into a cost function. In spite of the fact that these navigation systems are capable of guaranteeing the human safety during the robot navigation, they do not consider the information about social interaction such as human group and human–object interaction.

In contrast to the aforementioned human-aware mobile robot navigation systems, a few recent studies focus on machine learning-based human-aware robot navigation systems [44], [45], [46]. Luber *et al*. [44] proposed a socially aware robot navigation system. They first extracted human

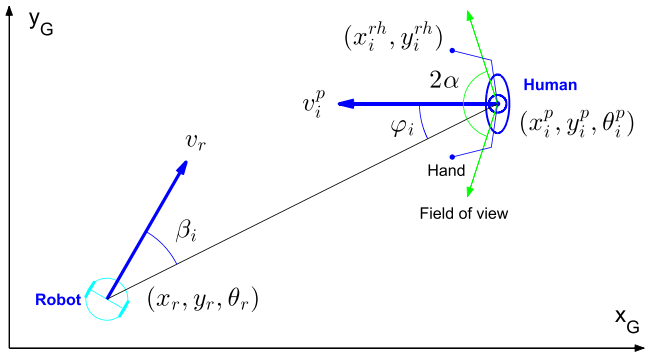

Fig. 1. Relative position between a person and a robot.

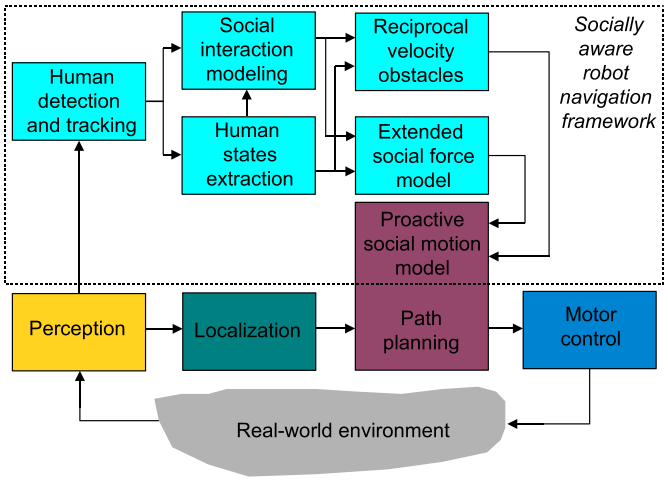

Fig. 2. Extended navigation scheme for mobile service robots is composed of two main parts: 1) a conventional navigation scheme and 2) a socially aware robot navigation framework (in cyan).

paths using observations of behavior in publicly available large-scale surveillance data sets. An unsupervised learning technique was then used to produce a set of relative motion prototypes for collision avoidance. However, the model is used only for a single interactive person. Beomjoon and Pineau [45] presented socially adaptive path planning based on inverse reinforcement learning for assistive robots. Although the algorithm generates a human-like trajectory using features extracted from the density and velocity of pedestrians and surrounding obstacles, state information about human social groups and human–object interactions has not been incorporated into the state features for the cost function of the local path planner. More recently, Kretzschmar *et al*. [46] proposed a socially compliant mobile robot navigation system, which allows a mobile robot to learn a model of the navigation behaviors of cooperatively navigating agents, such as pedestrians, using inverse reinforcement learning techniques.

III. Proactive Social Motion Model

Mobility is the most essential navigation issue of mobile robots. To allow a mobile robot to navigate safely in a real-world environment, the mobile robot must deal with typical functional blocks of the navigation system, including perception, localization, motion planning, and motion control as explained in [21]. However, such a conventional navigation scheme does not take human information and social constraints into account, so the mobile robot can only treat humans like regular obstacles. As a result, the robot is not capable of guaranteeing human comfort and safety during its navigation in social environments, especially in crowded and dynamic environments.

To ensure human safety and comfort when working in human–robot shared workspaces, mobile robots must distinguish humans from other obstacles, recognize human features from the socio-spatiotemporal characteristics of an individual human and a group of humans, and then incorporate such information into their navigation systems. To accomplish this, we propose an extended navigation scheme based on the conventional navigation scheme introduced in [21] by adding a socially aware mobile robot navigation framework.

Fig. 2 shows the new system architecture of the extended navigation scheme for mobile service robots in crowded and dynamic human environments. The navigation system consists of two major parts: 1) a conventional navigation scheme and 2) a socially aware robot navigation framework (in cyan). The conventional navigation scheme is typically based on the composition of four functional blocks: perception, localization, motion planning, and motion control. In the second part, the socially aware navigation framework aims to distinguish humans from regular obstacles, extracting the socio-spatiotemporal characteristics of humans in the vicinity of the robots for the development of the PSMM. The human detection and tracking block is used to detect and track humans in the real-world environment, while the social interaction modeling block is used to detect and identify social interactive information from human groups and human–object interactions. Both the ESFM and the HRVO use human states, including position, orientation, motion and hand poses, and social interactive information extracted by the robot vision system, to model the PSMM of the robot. The PSMM functions as a human-aware motion control framework for any local or global path planning in the motion planning system, and guarantees human safety and comfort by ensuring that the mobile robot exhibits socially acceptable behaviors in dynamic and crowded environments.

A. Human States, Robot States, and Relative Positions

We assume that there are N people appearing in the vicinity of the robot, $P = \{p_1, p_2, \ldots, p_N\}$, where p_i is the ith person. The human states of person p_i are represented as $p_i = (x_i^p, y_i^p, \theta_i^p, v_i^p, x_i^{rh}, y_i^{rh}, x_i^{lh}, y_i^{lh})$, where (x_i^p, y_i^p) is the position, θ_i^p is the orientation, v_i^p is the velocity, (x_i^{rh}, y_i^{rh}) is the right-hand position, and (x_i^{lh}, y_i^{lh}) is the left-hand position in the xy plane. Note that $\theta_i^p \in [-\pi, \pi]$. We define the state of the robot as $r = (x_r, y_r, \theta_r, v_r)$, where the position is (x_r, y_r), the orientation is θ_r, and the linear velocity is v_r. Fig. 1 shows an example of human states including human position, orientation, velocity, field of view, and hand poses; robot states including robot position, orientation, and velocity; and the relative pose between a person and a robot.

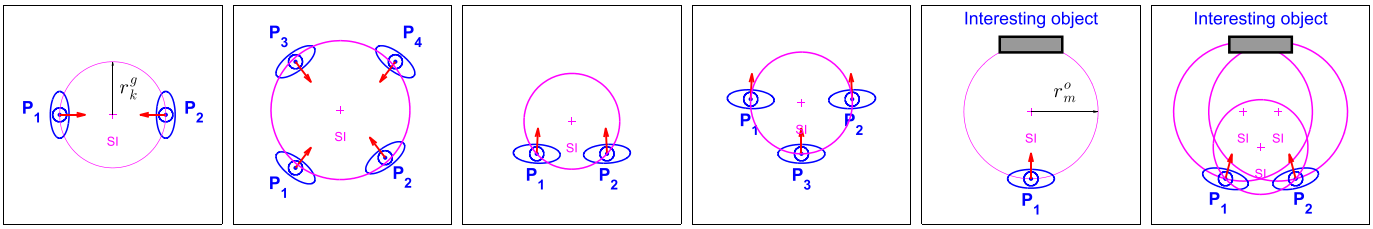

Fig. 3. Examples of the center and shape (magenta) of the social interaction spaces. (a) Group of two standing people. (b) Group of four standing people. (c) Group of two moving people. (d) Group of three moving people. (e) Human–object social interaction space. (f) Two human–object social interaction spaces.

B. Social Interaction Modeling

1) Human–Object Interaction: In a real-world environment, we pay more attention to the objects with which we interact, such as televisions, refrigerators, telephones, screens, and paintings. Thus, the robot needs to estimate human–object interaction, because this information is the key to defining an interaction space between humans and interesting objects.

We assume that a person $p_i = (x_i^p, y_i^p)$ is interacting with an interesting object $obj_j = (x_j^{\text{obj}}, y_j^{\text{obj}})$ as illustrated in Fig. 3(e). The set of parameters extracted from this human–object interaction space is $o_m = (x_m^o, y_m^o, r_m^o)$, where o_m is the mth human–object interaction space in the vicinity of the robot. (x_m^o, y_m^o) and r_m^o are the center point and the radius of the human–object interaction space, respectively, and are computed as follows:

$$(x_m^o, y_m^o) = \left(\frac{x_i^p + x_j^{\text{obj}}}{2}, \frac{y_i^p + y_j^{\text{obj}}}{2}\right) \tag{1}$$

$$r_m^o = \frac{\sqrt{(x_j^{\text{obj}} - x_i^p)^2 + (y_j^{\text{obj}} - y_i^p)^2}}{2}. \tag{2}$$

Note that the human–object interaction space is created by pairing a human and an interesting object. Fig. 3(f) shows an example of two human–object interaction spaces, in which two humans are interacting with an interesting object. In this example, two humans also form a human group that is studied in the next section.

2) Human Group Interaction: Findings in [20] show that 70% of humans intend to form interactive groups in social environments. Hence, detecting interactive human groups plays an essential role in the socially aware navigation framework. Methods for detecting social group interaction have been recently proposed [47], [48]. In this paper, we develop a human group detection technique that is modified from the graph cuts of F-formation (GCFF) algorithm [48].

Here, we briefly describe the original GCFF technique. The original GCFF technique was proposed for detecting social groups in still images using the formal definition of the F-formation described in [31] and the efficient graph-cut-based optimization [49]. The number of people in the vicinity of the robot $P = \{p_1, p_2, \ldots, p_N\}$ with corresponding poses $p_i = (x_i^p, y_i^p, \theta_i^p)$ are used as the inputs of this algorithm. In the graph formulation, the nodes are represented by individuals and the candidate o-space centers, while edges are defined between each pair of nodes of different type (i.e., between a transactional segment and a candidate o-space center). The authors modeled the probability of each individual belonging to a specific o-space, and then built the objective function by adding a minimum description length prior and considering the log function of the probability obtained. They also introduced an additive term that acts as the visibility constraint on the individual i regardless of the person j in a group that i is assigned to. The final objective function was defined as follows:

$$J(O_G|\text{TS}) = \sum_{i \in P} (u_{G_i} - x_{\mu_i})^2 + (v_{G_i} - y_{\mu_i})^2 + \sigma^{-2}|O_G| + \sum_{i,j \in P} R_{i,j}(O_{Gi}) \tag{3}$$

where $O_{G_i} = [u_{G_i}, v_{G_i}]$ represents the position of a candidate o-space center for an unknown F-formation $G_i = g$ containing i; $[x_{\mu_i}, y_{\mu_i}] = [x_i^p + Dcos(\theta_i^p), y_i^p + D\sin(\theta_i^p)]$ with D is the distance between the individual i and the center of its transactional segment; $O_g = [u_g, v_g]$ indicates the position of a candidate o-space center for F-formation $g \in \{1, K\}$ while $|O_G|$ is the number of distinct F-formations; and $R_{i,j}(O_{Gi})$ acts as a visibility constraint on i regardless of the person j in the group that i is assigned to. The output of the GCFF algorithm is the number of groups of humans. A detailed description of the method can be found in [48].

Unlike the original algorithm [48], instead of using only the spatial position and orientation information of static humans, we have used additional human motion information to make the model suitable for dynamic and crowded environments. A set of four parameters $p_i = (x_i^p, y_i^p, \theta_i^p, v_i^p)$ extracted from the spatial and temporal characteristics of humans in Section VII-B is used as the inputs for the GCFF technique. In other words, we added motion constraints into the objective function of the GCFF in (3), meaning that an individual is added into an F-formation if it has a similar velocity to all the other members in that F-formation. Equation (3) can be rewritten as follows:

$$J^{\text{new}}(O_G|\text{TS}) = J(O_G|\text{TS}) + \sum_{i,j \in P} V_{i,j}(O_{Gi}) \tag{4}$$

where

$$V_{i,j}(O_{Gi}) = \begin{cases} 0, & \text{if } v_i = 0, v_j = 0 \\ \exp(\beta|v_i - v_j|) - 1, & \text{otherwise} \end{cases} \tag{5}$$

where v_i and v_j are the velocities of the person i and j, respectively; $\beta > 0$ is the normalization factor of the human velocity; and $V_{i,j}(O_{Gi})$ acts as a velocity constraint on i regardless of the person j in the group that i is assigned to. Note that $V_{i,j}(O_{Gi}) = 0$ when $v_i = v_j$, and $V_{i,j}(O_{Gi}) > 0$ when $v_i \neq v_j$. The output of the algorithm is the number of human groups and its center point. To model the interaction space with these parameters, we used the circle fitting method [50] to find the center point and radius of each human group. Let $G = \{g_1, g_2, \ldots, g_K\}$ be the number of detected human groups in the vicinity of the robot; each social group interaction g_k has a set of parameters $g_k = (x_k^g, y_k^g, \theta_k^g, v_k^g, r_k^g)$, where (x_k^g, y_k^g) is the center point, θ_k^g is the orientation, v_k^g is the velocity, and r_k^g is the radius of the human group interaction. Note that if too many people exist in the robot's vicinity, we separate the large group into smaller groups of fewer than four people so that the robot can better deal with the dynamic situations of human groups. Fig. 3(a)–(d) shows an example of the human group detection algorithm for groups of two and four standing humans, and two and three moving humans, respectively.

C. Conventional Social Force Model

The conventional SFM [22] uses various attractive and repulsive forces to model both agent–agent and agent–object social force fields. These forces are based on both physical and psychological factors reflecting how agents avoid and approach each other. Formally, the SFM of an agent i is defined according to Newton's second law of motion

$$m_i \mathbf{a}_i(t) = \mathbf{F}_i^{sfm}(t) \tag{6}$$

where m_i is the mass, $\mathbf{a}_i(t)$ is the acceleration vector, and $\mathbf{F}_i^{sfm}(t)$ is the social force incorporated by the force vectors (attractive and repulsive forces) influencing the motion of agent i at time t.

1) Attractive Force to the Goal: Each agent i tends to move toward a desired direction $\mathbf{e}_i$ with a desired speed v_i^0, and thus the desired velocity $\mathbf{v}_i^0 = v_i^0 \mathbf{e}_i$. The desired velocity's direction is given by a vector pointing from the present position of the agent to the next goal, while the speed is selected so that the agent feels more comfortable. Let us assume that the agent's actual velocity at time t is $\mathbf{v}_i(t)$, and the $relaxation\ time\ K_i^{-1}$ is the time that agent i needs to adjust its actual velocity to the desired velocity. Therefore, the force attracting agent i to the goal is defined as follows:

$$\mathbf{F}_i^{\text{goal}} = K_i(\mathbf{v}_i^0 - \mathbf{v}_i(t)). \tag{7}$$

2) Repulsive Force From Other Agents: The agent i wants to maintain its desired velocity $\mathbf{v}_i^0$ toward the goal because of the attractive force $\mathbf{F}_i^{\text{goal}}$; however, its motion is also influenced by other agents j in its surrounding area. This influence is modeled as the repulsive force from agent j to agent i, and is defined as follows:

$$\mathbf{f}_{i,j} = A_i^a e^{\frac{(r_{i,j} - d_{i,j})}{B_i^a}} \mathbf{n}_{i,j} \tag{8}$$

where A_i^a and B_i^a are the strength and range of the repulsive force, respectively; $r_{i,j} = r_i + r_j$ is the sum of the radius of agent i and agent j; $d_{i,j}$ is the Euclidean distance between two agents; and $\mathbf{n}_{i,j}$ describes the unit vector pointing from agent j to agent i. The influence of the repulsive force is limited to the field of view of the agent; therefore, the anisotropic term is computed as follows:

$$w(\gamma_{i,j}) = \left(\lambda + (1-\lambda)\frac{1+\cos(\gamma_{i,j})}{2}\right) \tag{9}$$

where $\lambda \in [0, 1]$ is defined as the strength of the anisotropic factor, $\gamma_{i,j}$ is the relative direction of agent j with respect to the line through the centers of the foci of agents i and j. Finally, the repulsive forces $\mathbf{F}_i^a$ of all agents j in the vicinity of agent i are defined as follows:

$$\mathbf{F}_i^a = \sum_{j \neq i} A_i^a e^{\frac{(r_{i,j} - d_{i,j})}{B_i^a}} \mathbf{n}_{i,j} \left(\lambda + (1-\lambda)\frac{1+\cos(\gamma_{i,j})}{2}\right). \tag{10}$$

The primary set of parameters of the repulsive forces from other agents is $[A_i^a, B_i^a, \lambda]$.

3) Repulsive Force From Objects: In addition to the repulsive forces from other agents, the motion of agent i is also influenced by the repulsive forces from objects. Similar to the repulsive forces from other agents, the repulsive forces $\mathbf{F}_i^o$ of all objects $o \in O$ in the vicinity of agent i are defined as follows:

$$\mathbf{F}_i^o = \sum_{o \in O} A_i^o e^{\frac{(r_{i,o} - d_{i,o})}{B_i^o}} \mathbf{n}_{i,o} \left(\lambda + (1-\lambda)\frac{1+\cos(\gamma_{i,o})}{2}\right). \tag{11}$$

The primary set of parameters of the repulsive forces from objects is $[A_i^o, B_i^o, \lambda]$.

Ultimately, the SFM for agent i is synthesized by the force $\mathbf{F}_i^{\text{goal}}$ attracting it to the goal, the repulsive forces $\mathbf{F}_i^a$ from other agents j, and the repulsive forces $\mathbf{F}_i^o$ from objects o as follows:

$$\mathbf{F}_i^{\text{fsm}} = \mathbf{F}_i^{\text{goal}} + \mathbf{F}_i^a + \mathbf{F}_i^o. \tag{12}$$

The primary set of parameters of the conventional SFM is $[K_i, A_i^a, B_i^a, A_i^o, B_i^o, \lambda]$.

D. Extended Social Force Model

In the conventional SFM [22], the repulsive force from other agents presented in (10) uses only the relative position between agents. However, many other factors, such as human actions, social cues, and social constraints, influence the motion of the robot in dynamic and crowded environments. Hence, this information including relative positions, human actions, social cues, and social constraints should be incorporated into the socially aware navigation framework to ensure human comfort and safety, and to generate socially acceptable behaviors for the mobile robot. In this paper, we propose a new method that takes the socio-spatiotemporal characteristics of the humans including human body pose, field of view, hand poses, and social interactions consisting of human–object interaction and human group interaction into account to develop the ESFM. Fig. 5 shows an example of the social forces that influence the motion of the robot.

1) Human Body Pose-Based Repulsive Forces: The repulsive forces $\mathbf{F}_r^h$ based on all the humans in the vicinity of the robot can be computed using (10). The set of parameters of the human body-based repulsive forces is $[A_r^h, B_r^h, \lambda]$, where A_r^h and B_r^h are the strength and the range, respectively.

2) Object-Based Repulsive Forces: The repulsive forces $\mathbf{F}_r^o$ based on the objects in the robot's vicinity can be computed using (10). The set of parameters of the repulsive forces of the robot from objects o is $[A_r^o, B_r^o, \lambda]$, where A_r^o and B_r^o are the strength and the range, respectively.

3) Human Hand Pose-Based Repulsive Forces: To exploit the influence of the human hand poses of the person p_i on the robot's motion, we use the right-hand position (x_i^{rh}, y_i^{rh}) and left-hand position (x_i^{lh}, y_i^{lh}) in the xy plane. As a result, the repulsive forces of the left hand $\mathbf{F}_r^{lh}$ and the right hand $\mathbf{F}_r^{rh}$ of the people influencing the robot are computed using (10). The sets of parameters of the repulsive forces from the left hand and right hand are, respectively, $[A_r^h, B_r^{lh}, \lambda]$ and $[A_r^h, B_r^{rh}, \lambda]$, where the B_r^{lh} and B_r^{rh} values are computed as follows:

$$B_r^{lh} = B_r^h \frac{\sqrt{(x_i^{lh} - x_i^p)^2 + (y_i^{lh} - y_i^p)^2}}{r_h} \tag{13}$$

$$B_r^{rh} = B_r^h \frac{\sqrt{(x_i^{rh} - x_i^p)^2 + (y_i^{rh} - y_i^p)^2}}{r_h} \tag{14}$$

where r_h is the radius of the human body. As a result, the repulsive force based on the human hands is $\mathbf{F}_r^{hh} = \mathbf{F}_r^{lh} + \mathbf{F}_r^{rh}$.

4) Human–Object Interaction-Based Repulsive Forces: To take the human–object interaction into account for the ESFM, we propose a virtual human at the center of the human–object interaction space. Therefore, the repulsive force $\mathbf{F}_r^{ho}$ of the human–object interaction can be calculated using (10). The set of parameters of the repulsive forces from the human–object interaction is $[A_r^h, B_r^{ho}, \lambda]$, where B_r^{ho} is computed as follows:

$$B_r^{ho} = B_r^h \frac{r_m^o}{r_h} \tag{15}$$

where r_h is the radius of the human body and r_m^o is computed using (2).

5) Human Group-Based Repulsive Forces: Similar to the repulsive forces from the human–object interaction, the repulsive forces based on the social group of people $\mathbf{F}_r^{hg}$ are computed using (10). The set of parameters of the repulsive forces from the human group interaction is $[A_r^h, B_r^{hg}, \lambda]$

$$B_r^{hg} = B_r^h \frac{r_k^g}{r_h} \tag{16}$$

where r_h is the radius of the human body and r_k^g is computed in Section III-B2.

Ultimately, we integrate all the repulsive forces including: the human repulsive forces $\mathbf{F}_r^h$, the object repulsive forces $\mathbf{F}_r^o$, the human hands' repulsive forces $\mathbf{F}_r^{hh}$, the human–object repulsive forces $\mathbf{F}_r^{ho}$, and the human group repulsive forces $\mathbf{F}_r^{hg}$ to create the ESFM as in

$$\mathbf{F}_r^{\text{esfm}} = \mathbf{F}_r^h + \mathbf{F}_r^o + w_{hh}\mathbf{F}_r^{hh} + w_{ho}\mathbf{F}_r^{ho} + w_{hg}\mathbf{F}_r^{hg} \tag{17}$$

where $w_{hh}, w_{ho}, and\ w_{hg}$ are, respectively, the weights of the repulsive forces of the human hands, human–object interaction, and human group interaction. The set of parameters of the ESFM $\mathbf{F}_r^{\text{esfm}}$ is $[A_r^h, B_r^h, A_r^o, B_r^o, \lambda, w_{hh}, w_{ho}, w_{hg}]$.

E. Hybrid Reciprocal Velocity Obstacle Model

The HRVO method introduced in [23] is an extension of the RVO method [17]. The novelty of the HRVO is that it allows the robot to smoothly avoid humans, and reduce the possibility of oscillations of the robot motion. The HRVO has successfully been applied to multirobot collision avoidance [51]. This technique is a velocity-based approach [13] that takes the motion of other agents into account for collision avoidance in multiagent systems. HRVO can also be understood as a control policy where each agent selects a collision-free velocity from the 2-D velocity space in the xy plane. A construction of the HRVO of a robot and a human is illustrated in Fig. 4.

Suppose that a set of humans P and a set of dynamic and static obstacles O appear in the robot's vicinity. The combined HRVO for the mobile robot given in the existence of several humans and obstacles is the union of all the HRVOs induced by all the humans and the VOs induced by all the obstacles

$$\text{HRVO}_r = \bigcup_{h \in P} \text{HRVO}_{r|h} \cup \bigcup_{o \in O} VO_{r|o}. \tag{18}$$

According to [23], to avoid collisions with humans and objects, the velocity $\mathbf{v}_r^{\text{hrvo}}(t)$ of the robot is calculated as

$$\mathbf{v}_r^{\text{hrvo}}(t) = arg \min_{\mathbf{v}(t) \notin HRVO_r} \|\mathbf{v}(t) - \mathbf{v}_r^{\text{pref}}(t)\|_2 \tag{19}$$

where $\mathbf{v}_r^{\text{pref}}$ is computed as follows:

$$\mathbf{v}_r^{\text{pref}}(t) = v_r^{pref} \frac{\mathbf{p}_r - \mathbf{p}_r^{\text{goal}}}{\|\mathbf{p}_r - \mathbf{p}_r^{\text{goal}}\|_2} \tag{20}$$

where $\mathbf{p}_r$ is the current position, $\mathbf{p}_r^{\text{goal}}$ is the goal position, and v_r^{pref} is the preferred speed of the robot.

F. Hybrid Reciprocal Velocity Obstacle Based on Human States and Social Interactions

The conventional HRVO technique incorporates only the human pose and velocity into the model. In a social environment, however, human groups and human–object interactions are very common. Moreover, the motion of the robot is also affected by human action. Therefore, we incorporate this information into our proposed model to generate socially acceptable behaviors for the mobile robot. To do so, we add all the HRVOs induced by the human left hand, human right hand, human group, and human–object interaction into the union as in (18). Therefore, (18) is recalculated as follows:

$$\text{HRVO}_r^{\text{new}} = \text{HRVO}_r \cup \bigcup_{lh \in P} \text{HRVO}_{r|lh} \cup \bigcup_{rh \in P} \text{HRVO}_{r|rh} \cup \bigcup_{ho \in \text{HOI}} \text{HRVO}_{r|ho} \cup \bigcup_{hg \in \text{HGI}} \text{HRVO}_{r|hg} \tag{21}$$

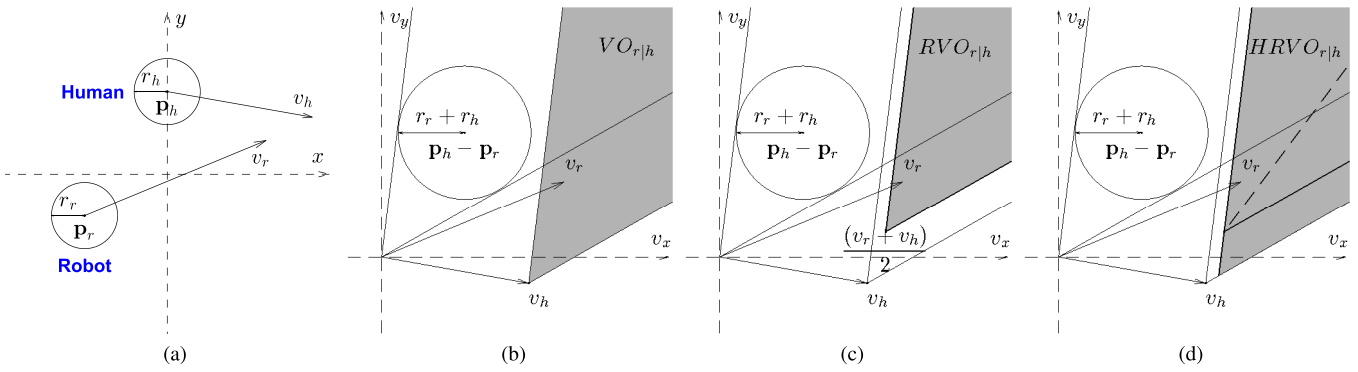

Fig. 4. Procedure of the HRVO of a robot and a human. (a) Configuration of a disk-shaped robot and a human in the xy plane with radii r_r and r_h, positions $\mathbf{p}_r$ and $\mathbf{p}_h$, and velocities v_r and v_h, respectively. (b) VO [13] for the robot induced by the human. (c) RVO [17] for the robot induced by the human. (d) HRVO [23] for the robot induced by the human.

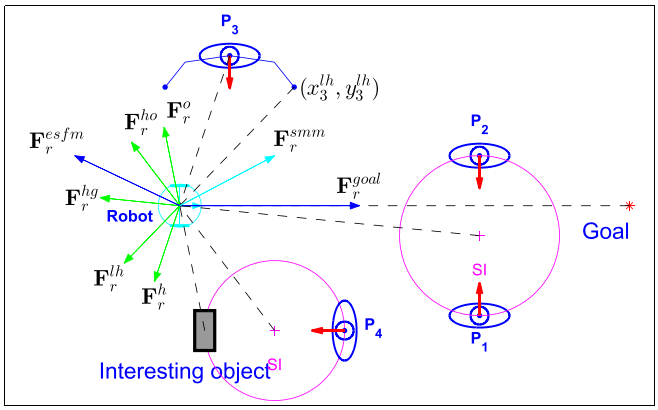

Fig. 5. Example of the social forces influencing the motion of a mobile robot: the extended social force $\mathbf{F}_r^{\text{esfm}}$, the attractive force to the goal $\mathbf{F}_r^{\text{goal}}$, and the final force affecting the motion of the robot $\mathbf{F}_r^{smm}$.

where HRVO_r is computed using (18); $\text{HRVO}_{r|lh}$ and $\text{HRVO}_{r|rh}$ are the HRVOs for the robot induced by the human left hand and the human right hand, respectively; $\text{HRVO}_{r|ho}$ is the HRVO for the robot induced by a human–object by a human–object interaction; and $\text{HRVO}_{r|hg}$ is the HRVO for the robot induced by a human group interaction. Note that P is the set of humans, O is the set of static and dynamic objects, HOI is the number of human–object interactions, and HGI is the number of human group interactions in the robot's vicinity.

G. Proactive Social Motion Model

The SFM works well in high density conditions with reasonable computational costs [22]. In addition, this technique provides a mechanism to incorporate human psychological factors such as social signals and social cues. However, this method is typically a type of reactive control, so it does not proactively deal with potential collisions when the robot is moving close to humans and obstacles [40]. In contrast, the HRVO, which is known as a velocity-based approach [13], has the advantage of proactive collision avoidance by taking the motions of humans and objects into account. But, it is difficult to directly incorporate social signals and social cues into this model. Therefore, to exploit the advantages of these techniques, we combine the ESFM with the HRVO so that the mobile robot is capable of socially dealing with human states and social constraints, and of proactively handling potential collisions with both humans and objects. Specifically, the robot velocity $\mathbf{v}_r^{\text{hrvo}}$ generated by the HRVO in (19) is used as the desired velocity $\mathbf{v}_i^0$ of the robot of the ESFM in (7). As a result, the attractive goal force $\mathbf{F}_r^{\text{goal}}$ and the total proactive social force $\mathbf{F}_r^{\text{psmm}}(t)$ influencing the robot motion are, respectively, computed as follows:

$$\mathbf{F}_r^{\text{goal}} = K_r^v(\mathbf{v}_r^{\text{hrvo}}(t) - \mathbf{v}_r(t)) \tag{22}$$

$$\mathbf{F}_r^{\text{psmm}}(t) = \mathbf{F}_r^{\text{goal}}(t) + \mathbf{F}_r^{\text{esfm}}(t) \tag{23}$$

where the *relaxation time* $(K_r^v)^{-1}$ is the time interval that the robot needs to adjust its actual velocity $\mathbf{v}_r(t)$ to the desired velocity $\mathbf{v}_r^{\text{hrvo}}$; and $\mathbf{F}_r^{\text{esfm}}$ is computed in (17). The PSMM of the mobile robot is computed as follows:

$$\mathbf{a}_r(t) = \frac{\mathbf{F}_r^{\text{psmm}}(t)}{m_r} \tag{24}$$

$$\mathbf{v}_r^{\text{new}}(t) = \mathbf{v}_r(t) + \mathbf{a}_r(t)dt \tag{25}$$

where $\mathbf{a}_r(t)$ and m_r are the acceleration and mass of the robot, respectively; $\mathbf{v}_r(t)$ is the current velocity of the robot; dt denotes the time interval; and $\mathbf{v}_r^{\text{new}}(t)$ is the velocity command that is then incorporated into the motion planning system.

IV. Incorporating the Proactive Social Motion Model Into Motion Planning

Once the velocity command $\mathbf{v}_r^{\text{new}}(t)$ of the mobile robot has been computed using (25), the control command of the robot is calculated to drive the robot to proactively and socially avoid the humans, human group social interaction space, human–object social interaction space, and obstacles. In this paper, we apply the velocity command to a robot model consisting of a two-wheel differential drive mobile robot platform with two additional castor wheels. We define the state of the robot $r(t) = (x_r(t), y_r(t), \theta_r(t))$ at time t, with position $(x_r(t), y_r(t))$, and orientation $\theta_r(t)$. The state of the robot at time $(t+1)$ is governed by the

following equations:

$$\begin{bmatrix} x_r(t+1) \\ y_r(t+1) \\ \theta_r(t+1) \end{bmatrix} = \begin{bmatrix} x_r(t) \\ y_r(t) \\ \theta_r(t) \end{bmatrix} + \begin{bmatrix} \frac{v_r^r + v_r^l}{2} \cos(\theta_r(t))dt \\ \frac{v_r^r + v_r^l}{2} \sin(\theta_r(t))dt \\ \frac{v_r^r - v_r^l}{L} dt \end{bmatrix} \quad (26)$$

where v_r^r and v_r^l are the linear velocity commands of the right and left wheels of the robot, respectively, and L denotes the wheelbase of the robot.

Suppose that the velocity command $\mathbf{v}_r^{\text{new}}(t) = (v_r^x(t), v_r^y(t))$, and the preferred orientation of the robot is $\theta_r^{\text{pref}}(t) = atan2(v_r^y(t), v_r^x(t))$. The following equations are used to compute v_r^r and v_r^l:

$$v_r^r = \|\mathbf{v}_r^{\text{new}}(t)\|_2 + K_r^\theta \frac{L(\theta_r^{\text{pref}}(t) - \theta_r(t))}{2} \quad (27)$$

$$v_r^l = \|\mathbf{v}_r^{\text{new}}(t)\|_2 - K_r^\theta \frac{L(\theta_r^{\text{pref}}(t) - \theta_r(t))}{2} \quad (28)$$

where $(K_r^\theta)^{-1}$ is the time interval that the robot needs to adjust its current orientation $\theta_r(t)$ to the preferred orientation $\theta_r^{\text{pref}}(t)$. Substituting the new high-level control inputs from (27) and (28) into (26), we obtain the proactive social motion controller for the socially aware robot navigation framework. This can be used with any path planning method (even a set of waypoints) to navigate the robot toward a destination while socially and safely avoiding humans, and taking into account human group social interactions, and human–object social interaction in a socially acceptable manner

$$\begin{bmatrix} x_r(t+1) \\ y_r(t+1) \\ \theta_r(t+1) \end{bmatrix} = \begin{bmatrix} x_r(t) \\ y_r(t) \\ \theta_r(t) \end{bmatrix} + \begin{bmatrix} \|\mathbf{v}_r^{\text{new}}(t)\|_2 \cos(\theta_r(t))dt \\ \|\mathbf{v}_r^{\text{new}}(t)\|_2 \sin(\theta_r(t))dt \\ K_r^\theta(\theta_r^{\text{pref}}(t) - \theta_r(t))dt. \end{bmatrix} \quad (29)$$

V. Human Comfortable Safety Indices

To validate the proposed socially aware robot navigation framework, we propose HCSIs using the proxemics-based personal space introduced in [30] and the F-formation definition of a social interactive human group proposed in [31]. The HCSI consists of three metrics: the *SII*, the *SGI*, and the *RMI*. The social individual and social group indices are used to measure the physical safety and comfort—psychological safety—of individuals, and human groups and human–object interactions, respectively. The RMI is used to measure the relative motion between a robot and a human. The combination of SII, SGI, and RMI values is used to measure socially acceptable behaviors in the mobile robot.

To use these indices to evaluate the physical and psychological safety of humans, and human group and human–object interactions, we define the radius of the human body r_h and the radius of the robot r_r. According to the concept of personal space under the proxemic model [30], the physical safety of a human is violated if the relative distance between a robot and a human is less than $d_p = r_h + r_r$. The psychological safety is disregarded if the relative distance between them is less than d_c, $d_c > d_p$. Note that d_c varies across cultures and is dependent on social situations and contexts. According to the F-formation of social interactive human groups [31], the psychological safety of a human group is violated if the robot moves beyond the circular boundary of human group interaction space with radius r_k^g [see Fig. 3(a)], because a human must approach this circular boundary if they wish to join the human group. Similar to the circle of social human group interaction, the human in a human–object interaction feels uncomfortable if a robot moves beyond the circular boundary of the human–object interaction space with radius r_m^o [see Fig. 3(e)]. The maximum velocities of the human $v_{\max}^p$ and the robot $v_{r\max}$ are also set, respectively, for the estimation of the RMI

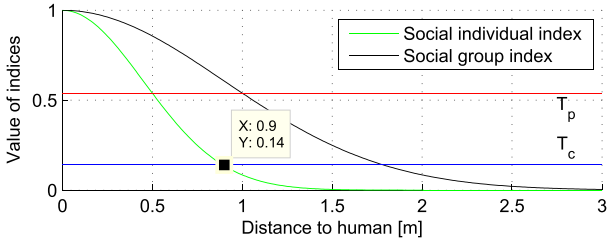

Fig. 6. Graph of the SII and SGI where $\sigma_0^p = 0.45$ and $\sigma_k^g = 0.9$.

$$\text{SII} = \max_{i=1:N} \exp\left(-\left(\left(\frac{x_r - x_i^p}{\sqrt{2}\sigma_0^p}\right)^2 + \left(\frac{y_r - y_i^p}{\sqrt{2}\sigma_0^p}\right)^2\right)\right). \quad (30)$$

A. Social Individual Index

SII value is calculated using (30), where (x_i^p, y_i^p) is the position of a human p_i, (x_r, y_r) denotes the position of a robot, σ_0^p is the standard deviation, and N is the number of humans in the vicinity of the robot. As the value of SII increases, the relative distance between the robot and the human decreases. The SII is equal to a physical threshold T_p—the highest value—when a robot crashes into a human: $((x_r - x_i^p)^2 + (y_r - y_i^p)^2)^{1/2} = d_p$. The $\sigma_0^p = \frac{d_c}{2}$ value is selected according to the Hall's personal space criterion [0.45, 1.2 m], so that the SII value is less than a psychological threshold T_c, which we consider as the threshold of psychological safety of humans, when the relative distance between the human and the robot is greater than d_c. As a result, a human feels less safe psychologically if the SII is greater than T_c. The value of SII with the corresponding distance between human and robot is shown in Fig. 6

$$\text{SGI} = \max_{k=1:K} \exp\left(-\left(\left(\frac{x_r - x_k^g}{\sqrt{2}\sigma_k^g}\right)^2 + \left(\frac{y_r - y_k^g}{\sqrt{2}\sigma_k^g}\right)^2\right)\right) \quad (31)$$

$$\sigma_k^g = \begin{cases} \frac{r_o^m}{2}, & \text{if human–object interaction} \\ \frac{r_k^g}{2}, & \text{if human group interaction.} \end{cases} \quad (32)$$

B. Social Group Index

SGI is calculated using (31) for human group interaction or human–object interaction. Here, σ_k^g is computed in (32); r_m^o and r_k^g are, respectively, computed in

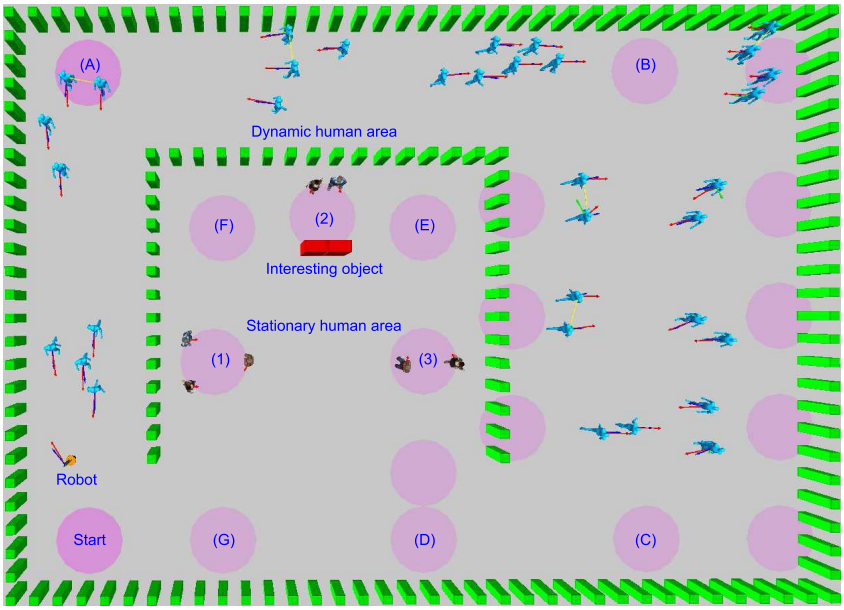

Fig. 7. Shopping mall-like simulated scenario consisting of walls, objects, humans, and social interactions. The scenario is composed of two main areas: a dynamic human area and a stationary human area. We deployed 41 humans and a mobile robot into the scenario. In the dynamic human area, the number of groups of moving humans was created randomly using a distributed function to generate the moving social group interactions. In the stationary human area, three social interactions were created including: 1) a group of three standing people; 2) a human–object interaction; and 3) a group of two standing people. The robot sequentially navigates from the start position (Start) through landmarks (A)–(G), and then returns to the start position while avoiding dynamic humans and human groups in the corridor-like dynamic human area, as well as social interaction situations in the shop-like static human area.

Sections III-B1 and III-B2; and K is the number of human groups or human–object interactions in the robot's vicinity. The range of SGI values is from 0.0 to 1.0. The SGI value decreases when the robot moves further from the center of the social space of a human group interaction (x_k^g, y_k^g) or a human–object interaction (x_m^o, y_m^o). This value is approximately equal to the psychological group threshold T_g when the relative distance between the robot and the center of the social interaction space is equal to the radius of the circle of the human group formation r_k^g, or the human–object formation r_m^o, as shown in Fig. 3. If the SGI value is greater than the psychological group threshold T_g, the humans in the human group or human–object interaction feel uncomfortable, that is, the robot behaviors do not guarantee the psychological safety aspects of the human group and human–object interactions. Fig. 6 shows an example of the SGI value corresponding to the distance between the robot and the center of the social interaction space

$$\mathrm{RMI} = \max_{i=1:N} \frac{2 + v_r \cos(\beta_i) + v_i^p \cos(\varphi_i)}{\sqrt{(x_i^p - x_r)^2 + (y_i^p - y_r)^2}}. \tag{33}$$

C. Relative Motion Index

RMI is used to measure the relative motion between a robot and a human, computed in (33). The parameters in (33) are shown in Fig. 1, where β_i is the angle between the robot orientation and the vector projected from the robot to the human p_i; φ_i is the angle between the human orientation and the vector projected from the human p_i to the robot; v_i^p and v_r are the velocities of person p_i and the robot, respectively; and N is the number of people. The RMI has a maximum value when a robot and a human are moving toward each other at the highest velocities at the closest distance d_p—the situation where the robot crashes into the human. The RMI value decreases when the velocities of the human and the robot decrease, and the relative distance and relative angle β_i and φ_i (see Fig. 1) between them increase. We define a motion threshold T_m of the RMI when a robot and a human are moving toward each other at the highest velocities at the distance d_c; the robot reaches the circular boundary of psychological safety of the human. As a result, the higher the value of RMI, the less socially acceptable the behavior of the robot.

VI. Simulation

We have chosen to implement and test our proposed method in the robot operating system (ROS) and visualized the result in Rviz—a visualization tool in ROS. We created a shopping mall-like scenario consisting of walls, interesting objects, static and dynamic humans, and social interactions for our experiments, as shown in Fig. 7.

A. Simulation Setup

In this paper, the PEDSIM library[1] and HRVO library[2] were inherited and modified to develop the ESFM and proposed PSMM. The simulation environment is developed based on the available software platform.[3] Note that we utilized only

[1] http://pedsim.silmaril.org

[2] http://gamma.cs.unc.edu/software/

[3] Designed by the Social Robotics Laboratory, University of Freiburg, Germany, https://github.com/srl-freiburg

TABLE I
PARAMETERS SET IN EXPERIMENTS

Parameter	Value	Parameter	Value	Parameter	Value
A_r^h	2.1	B_r^h	0.35	A_r^o	10
B_r^o	0.8	λ	0.45	w_{hh}	1.0
w_{ho}	1.0	w_{hg}	1.0	K_r^v	2.0
K_r^θ	2.0	r_r	0.25[m]	r_h	0.25[m]
d_p	0.5[m]	d_c	0.9[m]	σ_0^p	0.45
T_p	0.54	T_c	0.14	T_g	0.14
T_m	2.2	$v_{r_{max}}$	1[m/s]	v_{max}^p	1[m/s]

the conventional SFM, the function to add individual humans, groups of moving humans, objects, and walls in this software platform. Using this software platform, we developed a shopping mall-like environment, added humans, social interaction situations, and interesting objects for our demonstration. We then incorporated the social group modeling, the ESFM, the HRVO, and the PSMM into this simulation environment.

For each experiment, the robot was planned to navigate from the start position (Start) through landmarks (A)–(G), and then to return to the start position while dealing with social situations and human contexts, human–object interactions, and human groups. A total of 41 humans are deployed in the scenario. In the stationary human area, three social interactions are created, including: 1) a group of three standing people; 2) a human–object interaction—a group of two people looking at an interesting object; and 3) a group of two standing people. In the dynamic human area, the initial positions of the moving humans are randomly distributed in the scenario, and their initial velocities are set at 0.0 m/s. The maximum velocity of each human is set to 1.0 m/s and their actual velocities are randomly generated using a normal distribution function $\mathcal{N}(0.8, 0.2)$, where the mean and the standard deviation of the human's velocity are 0.8 and 0.2, respectively, that is, the human's velocity is randomly selected around 0.8 m/s. We also generated numerous social group interactions of two moving humans using a normal distribution function $\mathcal{N}(7, 2)$, where the mean and the standard deviation of the number of the social group interaction are 7 and 2, respectively, that is, the number of the social group interactions is randomly selected around seven interactive groups for each simulation. Note that all the human behaviors are equipped with either the SFM or the PSMM to ensure that human behaviors are either reactive or proactive to moving objects like natural human movements. Their positions are randomly initialized for their movement routines in the scenario. To get empirical data, we executed the robot in a loop until more than 70 000 samples were archived (each sample corresponding to a time step)—more than 22 rounds in the scenario.

We experimented with the set of parameters selected according to the definition of personal space in Hall's model [30] and our empirical experiences of this robot platform as shown in Table I. Specifically, we chose the radius of the human body $r_h = 0.25$ m and the radius of the robot body $r_r = 0.25$ m, corresponding to the relative distance $d_p = 0.5$ m for the physical safety of humans. We chose the relative distance $d_c = 0.9$ m for the psychological safety of humans. Human psychological safety is assured if the SII value is smaller than the threshold $T_c = 0.14$ (i.e., the relative distance between the human and the robot is greater than 0.9 m). In contrast, human physical safety is violated—the robot crashes into the human—if the SII value is greater than the psychological threshold $T_p = 0.54$ (the relative distance between them is smaller than 0.5 m). The SGI value is equal to 1.0 when the robot navigates across the center of the social interaction space. The psychological safety of humans in a human group interaction or a human–object interaction is guaranteed if the SGI value is less than the psychological group threshold $T_g = 0.14$, that is, the robot navigates outside the circular boundary of social interaction spaces (see Fig. 3). We empirically chose the maximum velocity of humans $v_{max}^p = 1.0$ m/s and the robot $v_{r_{max}} = 1.0$ m/s so that the maximum value of the RMI is 8.0 when the robot and the human are moving toward each other at their highest velocities at the closest distance $d_p = 0.5$ m. The RMI value decreases when the velocities of the human and the robot decrease, and the relative distance and the relative orientation β_i and φ_i between them increase. Note that the motion threshold of the RMI T_m is 2.2 where the relative distance between the human and the robot $d_c = 0.9$ m, the human velocity $v_i^p = 0$, and the robot velocity $v_r = 0$.

B. Simulation Results

To demonstrate the effectiveness and usefulness of the proposed method, we have implemented three experiments to compare our PSMM with the conventional SFM using the HCSIs presented in Section V. We also conducted statistical analysis of all the experiments to illustrate the effectiveness of our method. A video clip of our simulation results can be found at this link.[4]

1) Simulation 1 (SFM–SFM): First, we examined the robot's behaviors when the robot motion model and humans were equipped with SFM. The SII, SGI, and RMI are shown in Fig. 8(a), (d), and (g), respectively. The SII values higher than the psychological threshold $T_c = 0.14$ and those higher than the physical threshold $T_p = 0.54$ (existing in simulation only) indicate that the robot moved too close to the humans several times, and even crashed into them; thus, physical safety and psychological safety were not satisfied. The SGI values were much greater than those for psychological group safety $T_g = 0.14$, implying that the robot crossed through the social interaction spaces between the human groups and human–object interactions, leading to human discomfort in social interactive situations and contexts. In addition, the RMI values being higher than the motion threshold $T_m = 2.2$ show that the robot moved too close to the humans, instead of proactively and socially avoiding them.

2) Simulation 2 (PSMM–SFM): Next, we studied the robot's behaviors when the robot motion model was installed with the proposed PSMM while humans were equipped with the SFM. The SII values, SGI values, and RMI values are,

[4]https://youtu.be/6mqPzCjRZAc

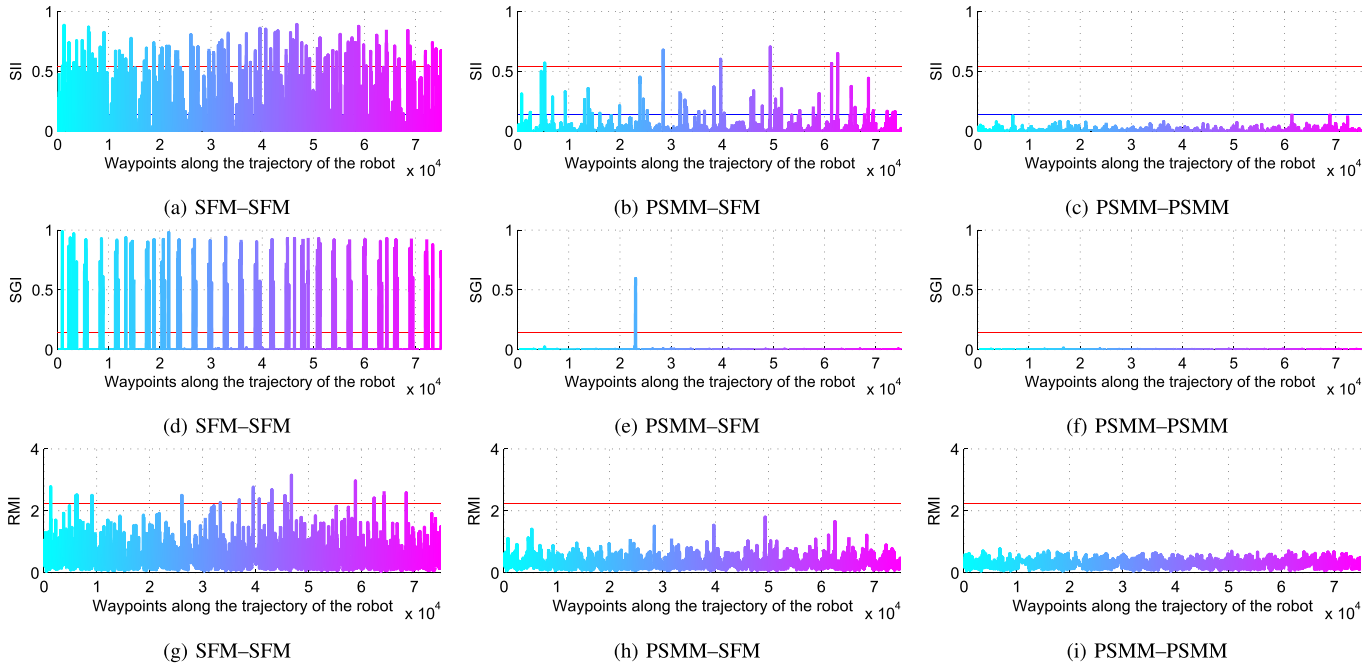

(a) SFM–SFM (b) PSMM–SFM (c) PSMM–PSMM

(d) SFM–SFM (e) PSMM–SFM (f) PSMM–PSMM

(g) SFM–SFM (h) PSMM–SFM (i) PSMM–PSMM

Fig. 8. HCSIs of three simulations (three pairs). The HCSI values of simulation 1—SFM–SFM, simulation 2—PSMM–SFM, and simulation 3—PSMM–PSMM are, respectively, presented in the first column—SII, the second column—SGI, and the third column—RMI.

respectively, shown in Fig. 8(b), (e), and (h). The SII values were sometimes higher than the psychological threshold $T_c = 0.14$, and were even higher than the physical threshold $T_p = 0.54$, because the robot could not actively avoid humans when individuals or human groups intended to move toward it. However, the density of the SII values that were higher than T_p and T_c shown in Fig. 8(b) was much less than that of the SII values shown in Fig. 8(a), indicating that a robot equipped with the PSMM better maintained physical and psychological safety than a robot equipped with the SFM. The SGI values were mostly maintained lower than the psychological group threshold $T_g = 0.14$, except that the SGI value reached 0.58, where the robot was heading to a destination while a group of two people were leaving from the same destination. The SII and SGI values also show that the robot inconsistently navigated in a socially acceptable manner. The RMI values were maintained lower than the motion threshold $T_m = 2.2$, that is, the robot proactively avoided humans.

3) Simulation 3 (PSMM–PSMM): Finally, we investigated the robot's behaviors when both the robot and the humans were equipped with the same proposed PSMM. The SII, SGI, and RMI values are, respectively, shown in Fig. 8(c), (f), and (i). The SII values were always maintained lower than the psychological threshold $T_c = 0.14$, while the SGI values were maintained at approximately 0.0, much lower than the psychological group threshold $T_g = 0.14$, that is, both the physical and psychological safety aspects were satisfied and the robot navigated in a socially acceptable manner. The RMI values shown in Fig. 8(i) were maintained at lower than the motion threshold $T_m = 2.2$, even lower than the RMI shown in Fig. 8(h), that is, the robot proactively acted according to human behaviors. Therefore, we believe that humans feel more comfortable when both the robot and humans follow the given rules of PSMM in social environments.

C. Statistical Analysis of the Simulation Results

In this section, we analyze the robot behaviors through the statistical data collected from 70 000 samples for each experiment. Using the psychological threshold T_c of the SII value, the psychological group threshold T_g of the SGI value, and the relative motion threshold T_m of the RMI value as the baselines, we qualitatively verify how the PSMM performs in comparison with the conventional SFM. The statistical data help us to verify whether we can empirically select systematic parameters for the robot if we have good knowledge about human behaviors and their social environment as described in Section VI-A.

1) Percentage: Fig. 9 illustrates the percentage distributions of the SII, SGI, and RMI. Specifically, we take into account only the percentage calculated from the number of the robot's running steps satisfying the psychological threshold $T_c = 0.14$ of the SII, the psychological group threshold $T_g = 0.14$ of the SGI, and the relative motion threshold $T_m = 2.2$ of the RMI values. The percentages of the (SII, SGI, and RMI) indices of simulation 3 (PSMM–PSMM) are $(0.02, 0.00, 0.00)$, compared with $(8.87, 5.22, 0.08)$ in simulation 1 (SFM–SFM) and $(1.16, 0.10, 0.00)$ in simulation 2 (PSMM–SFM), respectively. These comparative results show that the robot and the humans equipped with the proposed PSMM had the smallest percentage, that is, the robot did not frequently move too close to the individuals and human groups when it was equipped with the PSMM. In other words, the robot *proactively and safely avoided* humans while navigating toward its given destination.

2) Mean and Standard Deviation of the Human Comfortable Safety Indices: The means and the standard deviations of the SII, SGI, and RMI values are shown in Fig. 10. The mean values of the SII and SGI in simulation 3 (PSMM–PSMM) are $(0.0027, 0.0001)$, compared with $(0.0387, 0.0275)$ in simulation 1 (SFM–SFM) and

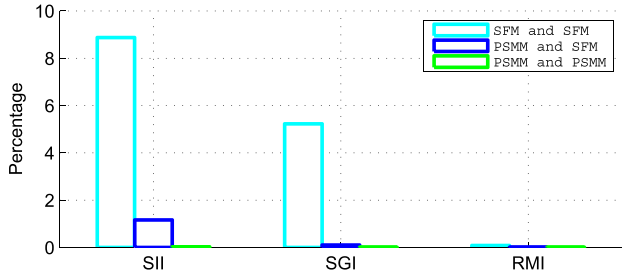

Fig. 9. Percentage of the samples that have values higher than the thresholds T_c, T_g, and T_m corresponding to SII, SGI, and RMI, respectively.

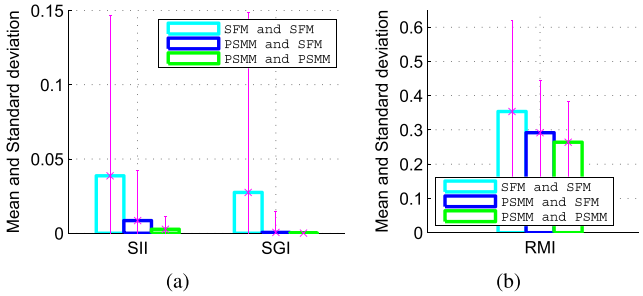

Fig. 10. Mean and standard deviation of the values of the SII and the SGI (a), and the RMI (b).

(0.0085, 0.0006) in simulation 2 (PSMM–SFM), respectively, that is, these values are the smallest mean when the robot and the humans are equipped with the proposed PSMM. The corresponding standard deviations of simulation 3 (0.0087, 0.0005) are smaller than those in simulation 1 (0.1082, 0.1210) and simulation 2 (0.0340, 0.0142), respectively. That means the robot with the PSMM did not navigate too close to the humans and human groups, so it behaved socially and safely to humans. Furthermore, the mean and standard deviation values of the RMI in simulation 3 are (0.2639, 0.1183), compared with (0.3535, 0.2658) in simulation 1 and (0.2919, 0.1521) in simulation 2, respectively. The comparative results of the means and standard deviations of the SII, SGI, and RMI indicate that, different from the robot behaviors when installed with the SFM, the robot equipped with the PSMM did not move too close to the individuals and the human groups at a high speed and at a small relative angle (see the relative pose in Fig. 1). Therefore, the robot *proactively planned its route to avoid* the humans when navigating toward its given destination.

3) Mean and Standard Deviation of Differentials of the Robot's Orientation and Velocity: To further demonstrate the proactiveness of the PSMM in terms of generating a smooth trajectory, so-called *proactively planned trajectory*, for the mobile robot in dynamic and crowded environments, we computed the mean and standard deviation of the differential of the robot's orientation and velocity between time steps (t) and $(t+1)$, as shown in Fig. 11. In simulation 3 (PSMM–PSMM), the values of the mean and the standard deviation of the differential of the robot's orientation and the velocity are (0.02, 0.2694) and (0.8653, 0.1607), compared with those in simulation 2 (PSMM-SFM) (0.0261, 0.3144)

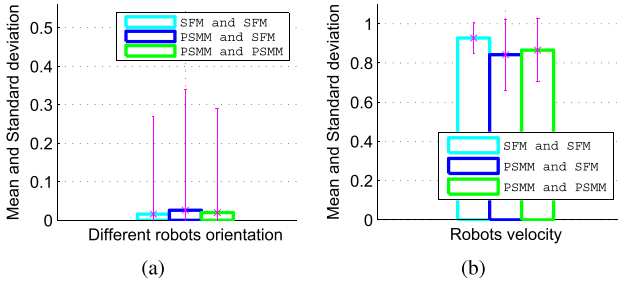

Fig. 11. Mean and standard deviation of the differential of the robot's orientation (a), and the robot's velocity (b) between time step t and $(t+1)$.

and (0.8422, 0.1805), respectively. We observed that the mean and standard deviation values of the robot's orientation in simulation 3 are smaller than those in simulation 2. Moreover, the mean value of the robot's velocity in simulation 3 is greater than that in simulation 2 while its corresponding standard deviation value in simulation 3 is smaller than that in simulation 2. These comparative results mean that the robot equipped with the PSMM navigated at higher velocity but did not need to rapidly change its navigation direction [measured by the differential of moving direction between time step (t) and $(t+1)$]. In addition, the robot did not change its orientation and velocity substantially. In contrast, the values of the mean and standard deviation of the differential of the robot's orientation and velocity in simulation 1 (SFM-SFM) are (0.0159, 0.2522) and (0.9273, 0.0806), respectively. These values indicate that the robot navigated at the highest velocity but did not change its direction smoothly, compared with those in simulations 2 and 3. The fact that the robot equipped with the SFM could not properly avoid the human groups and human–object interactions, and thus it did not guarantee human physical and psychological safety in dynamic and crowded environments.

Overall, the statistical analysis proves that the PSMM is capable of guaranteeing human safety and comfort in terms of both physical and psychological aspects, while allowing the mobile robot to proactively plan its smooth trajectory with socially acceptable behaviors through crowded and dynamic human environments. Moreover, we believe that the system parameters can be accordingly selected for our mobile robot platform in real-world experiment as presented in the following.

VII. Experiments

We have implemented the proposed framework on our mobile robot platform to validate its feasibility and effectiveness. To do that, we conducted experiments in an office-like environment to examine whether our robot could proactively avoid humans while navigating safely and socially in a real-world environment.

A. Mobile Robot Platform

We used an Eddie mobile robot platform equipped with a Microsoft Kinect sensor and a laser rangefinder, as shown in Fig. 12(a). The standard Kinect sensor composed of an

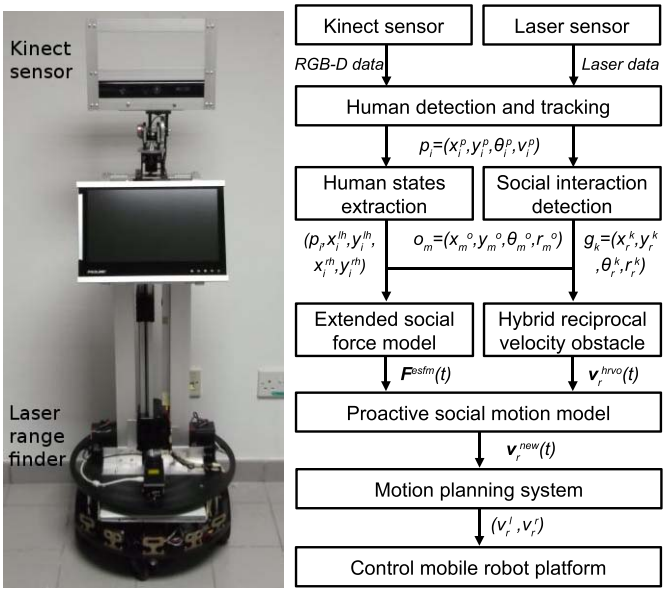

(a) (b)

Fig. 12. (a) Eddie mobile robot platform provided with a Kinect sensor and a laser range finder. (b) Data flow diagram of the proposed system.

infrared light projector, a depth sensor, an RGB camera, and a multiarray microphone was positioned at a 1.35 m height from the ground. The depth sensor range is from 0.8 to 6.0 m with a vertical viewing angle of 43° and a horizontal viewing angle of 57°. This low-cost hardware can provide RGB-D data with 640 × 480 pixels resolution at a maximal frame rate of 30 frames/s. The laser range finder, UGR-04LX-UG01 positioned at a height of 0.4 m, provides distance measurements up to 6.0 m in the angular field of view 240°.

B. Human Detection and Tracking, and Extraction of Human States

The human detection and tracking module provides an important input for the remaining modules in our proposed framework. However, the main focus of this paper is to propose a PSMM for mobile service robot in dynamic and crowded environments. Therefore, we adopted the result of the human detection and tracking system from [52] and [53]. We integrated two techniques for the experiments because the technique proposed in [52] provides us the 3-D pose of the humans but it is only used with the static camera, while the technique proposed in [53] can be used with the moving camera but it does not provide the 3-D human pose.

For Experiment 1 (avoiding stationary humans), we used the results from [52] to extract the 3-D human pose including human position, orientation, motion, and hand pose. Furthermore, to reduce the difficulty of estimating the gaze direction of humans over long distances, especially in dynamic environments, we used the human torso orientation information instead of the gaze direction. As a result, the human states extracted from the human states extraction model are $p_i = (x_i^p, y_i^p, \theta_i^p, v_i^p, x_i^{rh}, y_i^{rh}, x_i^{lh}, y_i^{lh})$. This information is then used as the inputs of the ESFM and HRVO models, as seen in Fig. 12(b).

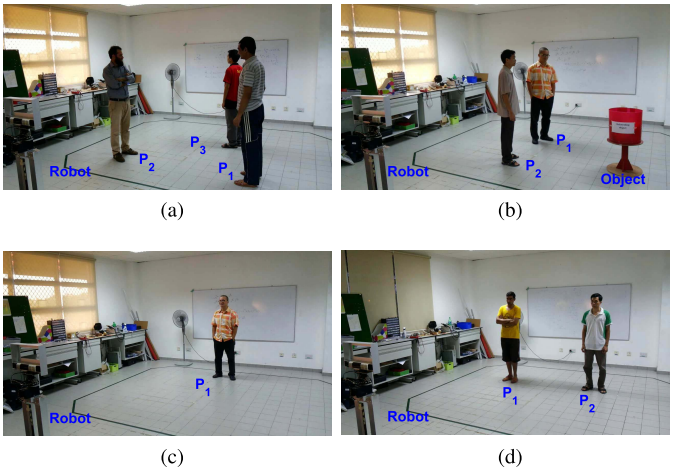

(a) (b) (c) (d)

Fig. 13. Experiment scenarios. (a) Three standing people. (b) Two people interacting with an object. (c) Walking person. (d) Group of two walking people.

For Experiment 2 (avoiding dynamic humans), we utilized the human detection and tracking algorithm developed in [53] to estimate the human position and velocity. The basic idea of this approach is to fuse the human information detected by laser data as presented in [54] and Kinect sensor data as explained in [55] using a particle filter. A detailed description of the technique can be found in [53]. As a result, the human states are $p_i = (x_i^p, y_i^p, \theta_i^p, v_i^p)$. This information is then used as the inputs of the social interaction modeling module, as shown in Fig. 12(b).

C. Experimental Setup

The data flow diagram of the proposed system in the mobile robot platform is shown in Fig. 12(b). The software core of the robot is developed on the ROS [56] run on an Intel core i7 2.2-GHz laptop. The proposed framework was implemented using the C++ programming language and MATLAB. We also used the OpenCV library [57] and the point cloud library [58].

In this paper, we conducted two experiments in our laboratory environment: Experiment 1—avoiding stationary humans and Experiment 2—avoiding dynamic humans. In each experiment, we verified the robot behavior in two cases: 1) SFM—using the conventional SFM introduced in [22] and 2) PSMM—using our proposed PSMM. We then compare the experimental results between these methods to illustrate the performance of the proposed framework. We executed all the experiments with the parameter values presented in Table I.

D. Experimental Results

1) Experiment 1 (Avoiding Stationary Humans): In this experiment, we aimed to examine whether the robot was able to avoid a stationary person or a group of standing people safely and comfortably. A video with our experimental results can be found at the hyperlinks.[5]

[5]https://youtu.be/vI6ovom97G0

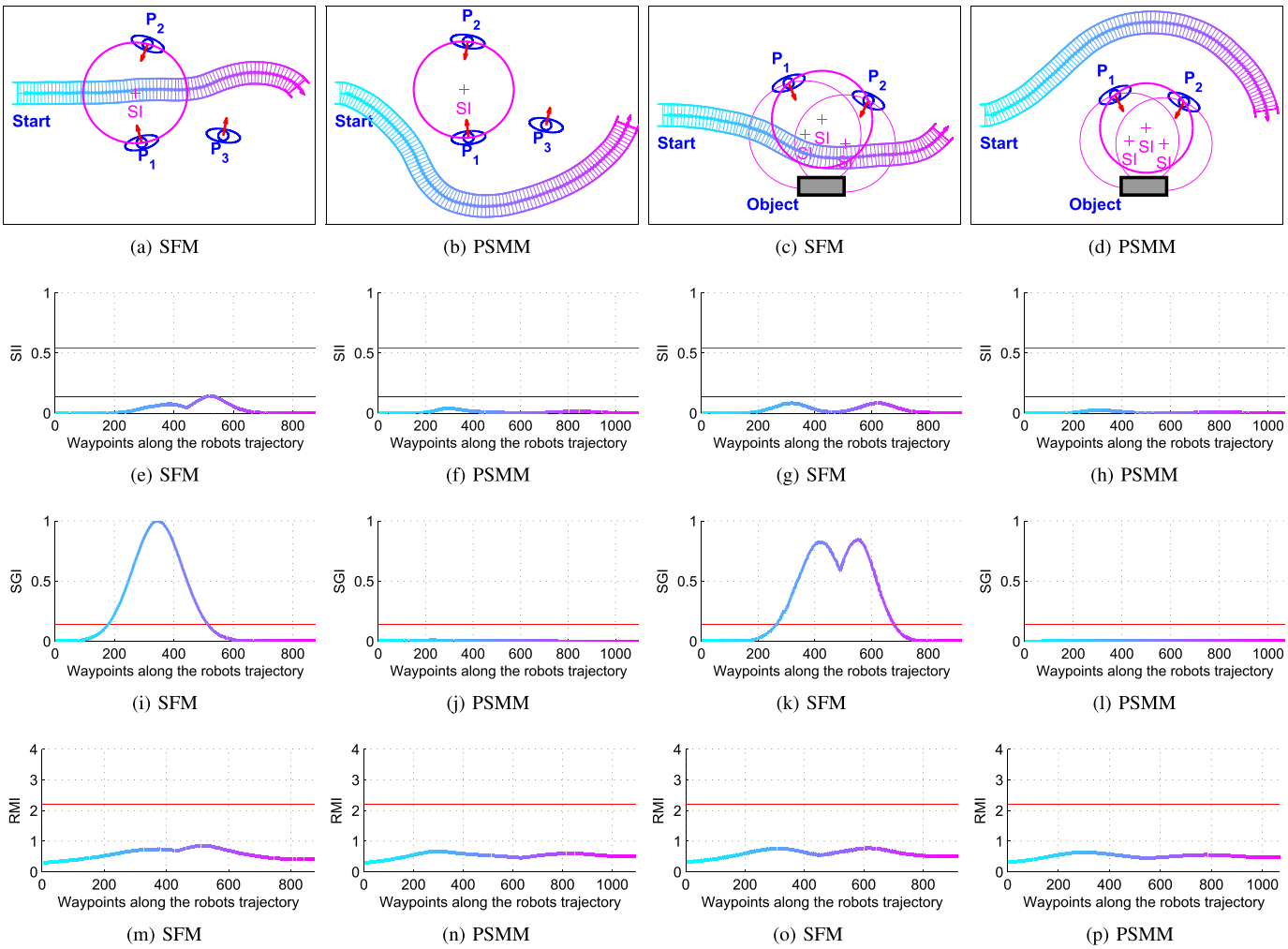

(a) SFM (b) PSMM (c) SFM (d) PSMM

(e) SFM (f) PSMM (g) SFM (h) PSMM

(i) SFM (j) PSMM (k) SFM (l) PSMM

(m) SFM (n) PSMM (o) SFM (p) PSMM

Fig. 14. Experimental results of Experiment 1—robot avoids stationary people, including: 1) a group of three standing people and 2) two human–object interactions. Two cases studied are examined: SFM—the robot is equipped with the conventional SFM and PSMM—the robot is equipped with the proposed PSMM. The first row shows the trajectory of the robot and the human. The second, third, and fourth rows illustrate the HCSIs including the SII, SGI, and RMI, respectively.

a) Avoiding a standing person and a group of two standing people: The scenario was set up as seen in Fig. 13(a), in which three people were positioned in the field of view of the robot. The people p_1 and p_2 formed a group while the person p_3 stood alone. The experimental results of the SFM are shown in Fig. 14(a), (e), (i), and (m), and the experimental results of the PSMM are shown in Fig. 14(b), (f), (j), and (n). As shown in Fig. 14(a), although the robot did not navigate too close to the people, it crossed through the interaction space between the people p_1 and p_2 so these people might not feel comfortable. In contrast, the robot socially and politely moved around the group of two people p_1 and p_2 and avoided the person p_3 socially and respectively, as seen in Fig. 14(b).

b) Avoiding a group of two people interacting with an object: The scenario was set up as seen in Fig. 13(b), in which a group of two standing people interacting with an interesting object were positioned in the field of view of the robot. The experimental results of the SFM are shown in Fig. 14(c), (g), (k), and (o), and the experimental results of the PSMM are shown in Fig. 14(d), (h), (l), and (p). As shown in Fig. 14(c), although the robot did not navigate too close to the people, it crossed through the interaction space between the people p_1 and p_2, and also the interaction space between the people and the object, and thus these people might not feel comfortable, e.g., when they were watching TV. In contrast, the robot respectively and socially moved around the group of two people p_1 and p_2, as seen in Fig. 14(d).

The experimental results shown in Fig. 14 illustrate that the robot equipped with our proposed PSMM proactively guided the mobile robot to avoid not only a standing person but also a group of standing people and a human–object interaction in socially acceptable manners, which could not be done by the conventional SFM.

2) Experiment 2 (Avoiding Dynamic Humans): In the second experiment, we aimed to examine whether the robot was able to avoid a dynamic person or a group of dynamic people safely and comfortably. A video with our experimental results can be found at the hyperlinks.[6]

a) Avoiding a walking person: The scenario was set up as seen in Fig. 13(c), in which a walking person was positioned in the field of view of the robot. The experimental results of the SFM are shown in Fig. 15(a), (e), (i), and (m),

[6]https://youtu.be/lyK2vLSeaHE

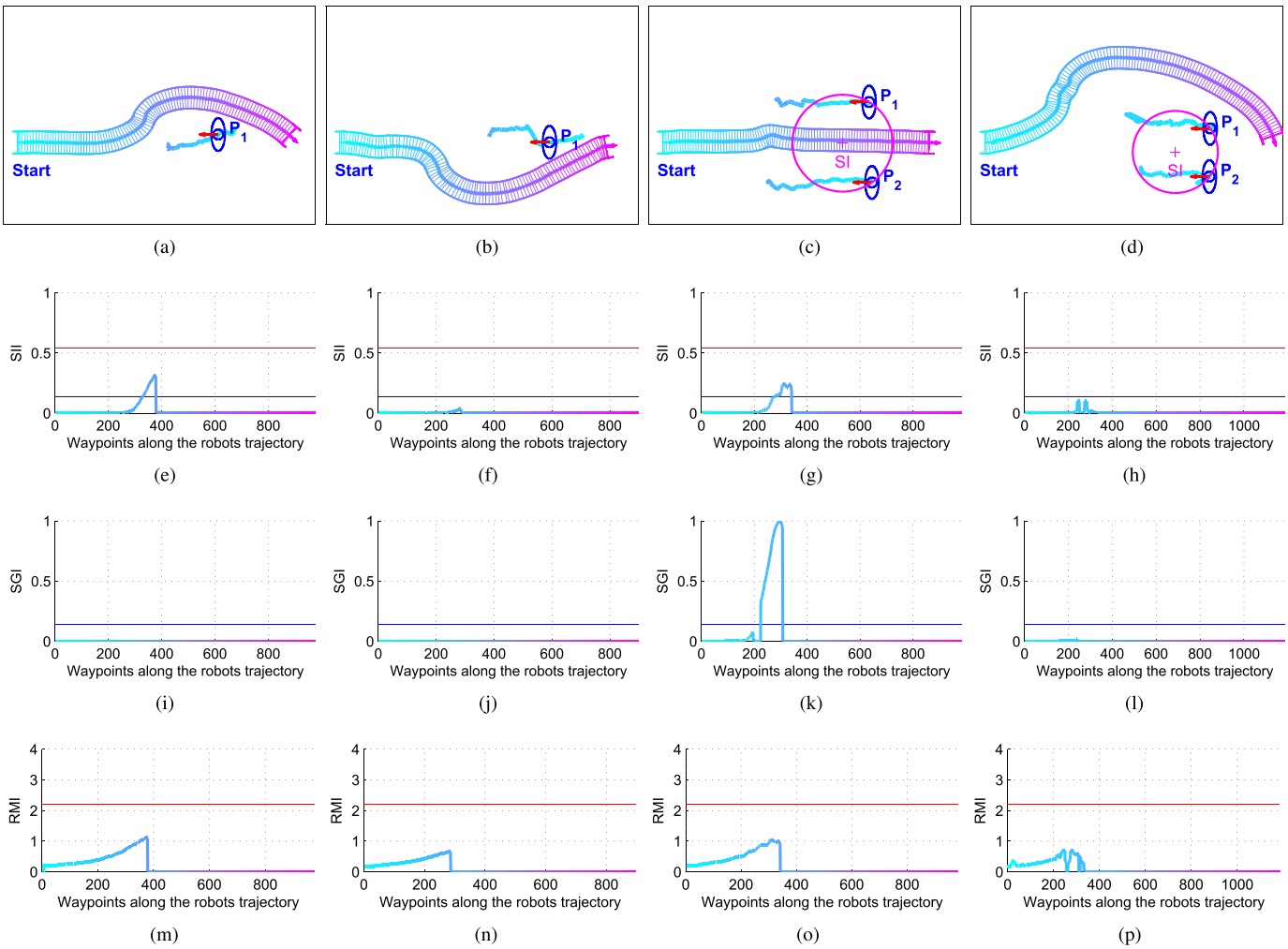

Fig. 15. Experimental results of Experiment 2—robot avoids dynamic people, including: 1) a moving person and 2) a group of two moving people. Two cases studied are examined: SFM—the robot is equipped with the conventional SFM and PSMM—the robot is equipped with the proposed PSMM. The first row shows the trajectory of the robot and the human (a), (b), (c), (d). The second (e), (f), (g), (h), third (i), (j), (k), (l), and fourth (m), (n), (o), (p) rows illustrate the HCSIs including the SII, SGI, and RMI, respectively.

whereas the experimental results of the PSMM are shown in Fig. 15(b), (f), (j), and (n). As shown in Fig. 15(a), although the robot did not collide with the person p_1, it only started avoiding the person at the short distance, and thus the moving person p_1 might not feel comfortable with this robot navigation. In contrast, the robot proactively avoid the walking person p_1, as seen in Fig. 15(b).

b) Avoiding a group of two walking people: The scenario was set up as seen in Fig. 13(d), in which a group of two walking people were positioned in the field of view of the robot. The experimental results using the SFM are shown in Fig. 15(c), (g), (k), and (o), and the experimental results with the PSMM are shown in Fig. 15(d), (h), (l), and (p). As shown in Fig. 15(c), although the robot still ensured the human physical safety because it did not navigate too close to the people, it crossed through the interaction space between the people p_1 and p_2, so these people might not feel comfortable. In contrast, the robot respected the group interaction space of two people p_1 and p_2 and proactively moved around the group to not interfere their social interaction, e.g., when they were in a social conversation, as seen in Fig. 15(d).

Overall, the experimental results shown in Figs. 14 and 15 illustrate that the robot equipped with the PSMM enabled the mobile robot to proactively avoid not only a static human and a human group but also a dynamic human and human group, providing comfortable safety for the humans and socially acceptable behaviors for the robot.

VIII. Conclusion

We have presented a PSMM for the socially aware navigation framework of mobile service robots in dynamic and crowded human environments. In our model, the socio-spatiotemporal characteristics of humans and human groups are taken into account to develop the PSMM for the mobile robot by taking advantages of both the ESFM and the HRVO. We have demonstrated the effectiveness of the proposed method through both simulations and real-world experiments. We emphasize that the newly developed PSMM can be incorporated into any path planning method to make a human-

aware motion planning system that is capable of dealing with different social situations and contexts of humans and human groups to generate a proactively planned trajectory for a mobile service robot in crowded and dynamic environments. We conclude that the PSMM is capable of enabling a mobile robot not only to navigate safely and socially but also to proactively plan its trajectory according to human and human groups in dynamic social environments with socially acceptable behaviors.

Our proposed PSMM has been developed on the background of HRVO and SFM models, which are known as proactive and reactive controllers for dynamic and crowded environments. Therefore, PSMM can be used for a very crowded and chaotic environment because new control commands are fast generated for the robot. Our major concern when applying the PSMM for a mobile service robot is about the robot perception because the computational cost of the human detection and tracking could dramatically increase at very crowded and chaotic environment, effecting to the real-time data processing of the PSMM. To make the robot to adapt to such environments, the maximum velocity of the robot should proportionally decrease. Therefore, robot perception and its computational complexity could be a limit that we should further investigate in the future.

Another focus of our future research directions is to examine how to incorporate more social signals and cues, and cultures rules into this PSMM to make a robot behave like humans in a social environment because the current PSMM enables the robot to avoid humans smoothly but does not always react like humans in terms of cultural rules, e.g., polite to give a way, following the right-hand-side traffic laws. In addition, we also think about how to incorporate the proposed PSMM with various path planners in social environments. In this paper, we used a set of waypoints, which are feasible in crowded and dynamic environments, but a path planner is necessary in a known environment. Incorporating a path planner and the PSMM to make a new motion planner is another interesting topic of our future research directions.

REFERENCES

[1] A. Y. Ng and S. J. Russell, "Algorithms for inverse reinforcement learning," in *Proc. 17th Int. Conf. Mach. Learn.*, 2000, pp. 663–670.

[2] A. Vinciarelli, M. Pantic, and H. Bourlard, "Social signal processing: Survey of an emerging domain," *Image Vis. Comput.*, vol. 27, no. 12, pp. 1743–1759, Nov. 2009.

[3] M. Pantic and A. Vinciarelli, *Social Signal Processing*, The Oxford Handbook of Affective Computing. Oxford, U.K.: Oxford Univ. Press, Dec. 2014.

[4] S. Thrun *et al.*, "MINERVA: A second-generation museum tour-guide robot," in *Proc. IEEE Int. Conf. Robot. Autom.*, vol. 3, May 1999, pp. 1999–2005.

[5] R. Triebel *et al.*, "SPENCER: A socially aware service robot for passenger guidance and help in busy airports," in *Proc. 10th Conf. Field Service Robot. (FSR)*, Toronto, ON, Canada, 2015, pp. 607–622.

[6] E. Marder-Eppstein, E. Berger, T. Foote, B. Gerkey, and K. Konolige, "The office marathon: Robust navigation in an indoor office environment," in *Proc. IEEE Int. Conf. Robot. Autom.*, May 2010, pp. 300–307.

[7] T. Kanda, M. Shiomi, Z. Miyashita, H. Ishiguro, and N. Hagita, "An affective guide robot in a shopping mall," in *Proc. 4th ACM/IEEE Int. Conf. Hum. Robot Interact.*, Mar. 2009, pp. 173–180.

[8] G. Ferrer, A. Garrell, and A. Sanfeliu, "Social-aware robot navigation in urban environments," in *Proc. Eur. Conf. Mobile Robots (ECMR)*, Sep. 2013, pp. 331–336.

[9] S. Nonaka, K. Inoue, T. Arai, and Y. Mae, "Evaluation of human sense of security for coexisting robots using virtual reality. 1st report: Evaluation of pick and place motion of humanoid robots," in *Proc. IEEE Int. Conf. Robot. Autom.*, vol. 3, Apr. 2004, pp. 2770–2775.

[10] O. Khatib, "Real-time obstacle avoidance for manipulators and mobile robots," in *Proc. IEEE Int. Conf. Robot. Autom.*, vol. 2, Mar. 1985, pp. 500–505.

[11] J. Borenstein and Y. Koren, "The vector field histogram-fast obstacle avoidance for mobile robots," *IEEE Trans. Robot. Autom.*, vol. 7, no. 3, pp. 278–288, Jun. 1991.

[12] D. Fox, W. Burgard, and S. Thrun, "The dynamic window approach to collision avoidance," *IEEE Robot. Autom. Mag.*, vol. 4, no. 1, pp. 23–33, Mar. 1997.

[13] P. Fiorini and Z. Shiller, "Motion planning in dynamic environments using velocity obstacles," *Int. J. Robot. Res.*, vol. 17, no. 7, pp. 760–772, 1998.

[14] S. M. LaValle and J. J. Kuffner, Jr., "Randomized kinodynamic planning," *Int. J. Robot. Res.*, vol. 20, no. 5, pp. 378–400, 2001.

[15] D. Hsu, R. Kindel, J.-C. Latombe, and S. Rock, "Randomized kinodynamic motion planning with moving obstacles," *Int. J. Robot. Res.*, vol. 21, no. 3, pp. 233–255, 2002.

[16] T. Fraichard and H. Asama, "Inevitable collision states. A step towards safer robots?" in *Proc. IEEE/RSJ Int. Conf. Intell. Robots Syst.*, vol. 1, Oct. 2003, pp. 388–393.

[17] J. van den Berg, M. Lin, and D. Manocha, "Reciprocal velocity obstacles for real-time multi-agent navigation," in *Proc. IEEE Int. Conf. Robot. Autom.*, Pasadena, CA, USA, May 2008, pp. 1928–1935.

[18] T. Kruse, A. K. Pandey, R. Alami, and A. Kirsch, "Human-aware robot navigation: A survey," *Robot. Auto. Syst.*, vol. 61, no. 12, pp. 1726–1743, Dec. 2013.

[19] J. Rios-Martinez, A. Spalanzani, and C. Laugier, "From proxemics theory to socially-aware navigation: A survey," *Int. J. Social Robot.*, vol. 7, no. 2, pp. 137–153, Sep. 2014.

[20] M. Moussaid, N. Perozo, S. Garnier, D. Helbing, and G. Theraulaz, "The walking behaviour of pedestrian social groups and its impact on crowd dynamics," *PLoS ONE*, vol. 5, no. 4, p. e10047, 2010.

[21] R. Siegwart, I. R. Nourbakhsh, and D. Scaramuzza, *Introduction to Autonomous Mobile Robots*. Cambridge, MA, USA: MIT Press, Feb. 2011.

[22] D. Helbing and P. Molnár, "Social force model for pedestrian dynamics," *Phys. Rev. E, Stat. Phys. Plasmas Fluids Relat. Interdiscip. Top.*, vol. 51, no. 5, pp. 4282–4286, May 1995.

[23] J. Snape, J. van den Berg, S. J. Guy, and D. Manocha, "The hybrid reciprocal velocity obstacle," *IEEE Trans. Robot.*, vol. 27, no. 4, pp. 696–706, Aug. 2011.

[24] S. Kyriacos *et al.*, "TERESA: A socially intelligent semi-autonomous telepresence system," in *Proc. IEEE Int. Conf. Robot. Autom. Workshop Mach. Learn. Social Robot.*, May 2015, pp. 1–5.

[25] T. Kruse, A. Kirsch, H. Khambhaita, and R. Alami, "Evaluating directional cost models in navigation," in *Proc. ACM/IEEE Int. Conf. Hum.-Robot Interact.*, 2014, pp. 350–357.

[26] D. V. Lu and W. D. Smart, "Towards more efficient navigation for robots and humans," in *Proc. IEEE/RSJ Int. Conf. Intell. Robots Syst.*, Nov. 2013, pp. 1707–1713.

[27] P. Trautman, J. Ma, R. Murray, and A. Krause, "Robot navigation in dense human crowds: The case for cooperation," in *Proc. IEEE Int. Conf. Robot. Autom.*, May 2013, pp. 2153–2160.

[28] L. Chi-Pang, C. Chen-Tun, C. Kuo-Hung, and F. Li-Chen, "Human-centered robot navigation—Towards a harmoniously human–robot coexisting environment," *IEEE Trans. Robot.*, vol. 27, no. 1, pp. 99–112, Feb. 2011.

[29] J. Rios-Martinez, A. Spalanzani, and C. Laugier, "Understanding human interaction for probabilistic autonomous navigation using risk-RRT approach," in *Proc. IEEE/RSJ Int. Conf. Intell. Robots Syst.*, Sep. 2011, pp. 2014–2019.

[30] E. T. Hall, *The Hidden Dimension: Man's Use Space Public Private*. London, U.K.: The Bodley Head Ltd, 1966.

[31] A. Kendon, *Conducting Interaction: Patterns Behavior Focused Encounters*. Cambridge, U.K.: Cambridge Univ. Press, 1990.

[32] J. V. Gómez, N. Mavridis, and S. Garrido, "Fast marching solution for the social path planning problem," in *Proc. IEEE Int. Conf. Robot. Autom.*, May 2014, pp. 1871–1876.

[33] R. Kirby, R. Simmons, and J. Forlizzi, "COMPANION: A constraint-optimizing method for person-acceptable navigation," in *Proc. IEEE Int. Symp. Robot Hum. Interact. Commun.*, Sep. 2009, pp. 607–612.

[34] E. A. Sisbot, L. F. Marin-Urias, R. Alami, and T. Simeon, "A human aware mobile robot motion planner," *IEEE Trans. Robot.*, vol. 23, no. 5, pp. 874–883, Oct. 2007.
[35] G. Ferrer, A. Garrell, and A. Sanfeliu, "Robot companion: A social-force based approach with human awareness-navigation in crowded environments," in *Proc. IEEE/RSJ Int. Conf. Intell. Robots Syst.*, Nov. 2013, pp. 1688–1694.
[36] P. Ratsamee, Y. Mae, K. Ohara, T. Takubo, and T. Arai, "Human–robot collision avoidance using a modified social force model with body pose and face orientation," *Int. J. Humanoid Robot.*, vol. 10, no. 1, p. 1350008, 2013.
[37] E. A. Sisbot, L. Marin-Urias, X. Broquère, D. Sidobre, and R. Alami, "Synthesizing robot motions adapted to human presence," *Int. J. Social Robot.*, vol. 2, no. 3, pp. 329–343, Sep. 2010.
[38] M. Svenstrup, S. T. Hansen, H. J. Andersen, and T. Bak, "Adaptive human-aware robot navigation in close proximity to humans," *Int. J. Adv. Robot. Syst.*, vol. 8, no. 2, pp. 7–21, 2011.
[39] M. Shiomi, F. Zanlungo, K. Hayashi, and T. Kanda, "Towards a socially acceptable collision avoidance for a mobile robot navigating among pedestrians using a pedestrian model," *Int. J. Social Robot.*, vol. 6, no. 3, pp. 443–455, Aug. 2014.
[40] F. Zanlungo, T. Ikeda, and T. Kanda, "Social force model with explicit collision prediction," *EPL (Europhys. Lett.)*, vol. 93, no. 6, p. 68005, 2011.
[41] D. Zhang, Z. Xie, P. Li, J. Yu, and X. Chen, "Real-time navigation in dynamic human environments using optimal reciprocal collision avoidance," in *Proc. IEEE Int. Conf. Mechatronics Autom.*, Aug. 2015, pp. 2232–2237.
[42] D. Claes, D. Hennes, and K. Tuyls, "Towards human-safe navigation with pro-active collision avoidance in a shared workspace," in *Proc. Workshop On-Line Decision-Making Multi-Robot Coordination (IROS)*, Hamburg, Gemany, Oct. 2015, pp. 1–8.
[43] J. van den Berg, S. Guy, M. Lin, and D. Manocha, "Reciprocal n-body collision avoidance," in *Robotics Research* (Springer Tracts in Advanced Robotics), vol. 70. Springer, 2011, pp. 3–19.
[44] M. Luber, L. Spinello, J. Silva, and K. O. Arras, "Socially-aware robot navigation: A learning approach," in *Proc. IEEE/RSJ Int. Conf. Intell. Robots Syst. (IROS)*, Oct. 2012, pp. 902–907.
[45] B. Kim and J. Pineau, "Socially adaptive path planning in human environments using inverse reinforcement learning," *Int. J. Social Robot.*, vol. 8, no. 1, pp. 51–66, Jan. 2015.
[46] H. Kretzschmar, M. Spies, C. Sprunk, and W. Burgard, "Socially compliant mobile robot navigation via inverse reinforcement learning," *Int. J. Robot. Res.*, vol. 35, no. 11, pp. 1289–1307, 2016.
[47] M. Cristani *et al.*, "Social interaction discovery by statistical analysis of F-formations," in *Proc. 22nd Brit. Mach. Vis. Conf.*, 2011, pp. 23.1–23.12.
[48] F. Setti, C. Russell, C. Bassetti, and M. Cristani, "F-formation detection: Individuating free-standing conversational groups in images," *PLoS ONE*, vol. 10, no. 5, p. e0123783, 2015.
[49] L. Ladický, C. Russell, P. Kohli, and P. H. S. Torr, "Inference methods for CRFs with co-occurrence statistics," *Int. J. Comput. Vis.*, vol. 103, no. 2, pp. 213–225, 2013.
[50] N. Chernov and C. Lesort, "Least squares fitting of circles," *J. Math. Imag. Vis.*, vol. 23, no. 3, pp. 239–252, Nov. 2005.
[51] D. Claes, D. Hennes, K. Tuyls, and W. Meeussen, "Collision avoidance under bounded localization uncertainty," in *Proc. IEEE/RSJ Int. Conf. Intell. Robots Syst. (IROS)*, Oct. 2012, pp. 1192–1198.
[52] P. NITE. (2011). [Online]. Available: http://www.openni.org
[53] X.-T. Truong, V. N. Yoong, and T.-D. Ngo, "RGB-D and laser data fusion-based human detection and tracking for socially aware robot navigation framework," in *Proc. IEEE Conf. Robot. Biomimetics*, Dec. 2015, pp. 608–613.
[54] K. O. Arras, O. M. Mozos, and W. Burgard, "Using boosted features for the detection of people in 2D range data," in *Proc. IEEE Int. Conf. Robot. Autom.*, Apr. 2007, pp. 3402–3407.
[55] M. Munaro, F. Basso, and E. Menegatti, "Tracking people within groups with RGB-D data," in *Proc. IEEE/RSJ Int. Conf. Intell. Robots Syst. (IROS)*, Oct. 2012, pp. 2101–2107.
[56] M. Quigley *et al.*, "ROS: An open-source robot operating system," in *Proc. ICRA Workshop Open Source Softw.*, vol. 32, 2009, pp. 151–170.
[57] G. Bradski, "The OpenCV Library," *Dr. Dobb's J. Softw. Tools Prof. Program.*, vol. 25, no. 11, pp. 120–123, 2000.
[58] R. B. Rusu and S. Cousins, "3D is here: Point cloud library (PCL)," in *Proc. IEEE Int. Conf. Robot. Autom.*, May 2011, pp. 1–4.

Xuan-Tung Truong received the B.Sc. degree in electrical and electronics engineering from the Faculty of Control Engineering, Le Quy Don Technical University, Hanoi, Vietnam, in 2007, the M.Sc. degree in computer engineering from the Embedded System Laboratory, Department of Computer Engineering and Information Technology, University of Ulsan, Ulsan, South Korea, in 2012, and the Ph.D. degree in computer science from the Faculty of Science, University of Brunei Darussalam, Bandar Seri Begawan, Brunei, in 2017. He is currently a Lecturer with the Faculty of Control Engineering, Le Quy Don Technical University. His research interests include human–robot interaction, socially aware robot navigation, robotics, computer vision, and machine learning.

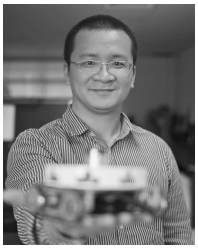

Trung Dung Ngo (M'07) received the B.Sc. degree in electronics and telecommunication from Vietnam National University, Hanoi, Vietnam, in 2000, the M.Sc. degree in computer systems engineering with a specialization in robotics from the University of Southern Denmark, Odense, Denmark, in 2004, and the Ph.D. degree in electrical and electronic engineering with a specialization in robotics from Aalborg University, Aalborg, Denmark, in 2008.

He was a Faculty Member of the Department of Electronic Systems, Aalborg University, and the Faculty of Science, University of Brunei Darussalam, Bandar Seri Begawan, Brunei. He is currently an Associate Professor with the University of Prince Edward Island, Charlottetown, PE, Canada, where he is the Founding Director of the More-Than-One Robotics Laboratory and the Lead Researcher of the Center for Excellence in Robotics and Industrial Automation. His research interests include multirobot systems, modular robotics, and human–robot cooperation.